arXiv:2006.16770v1 [math.AP] 30 Jun 2020

THE INVERSE-DEFORMATION APPROACH TO FRACTURE

PHOEBUS ROSAKIS[1,2], TIMOTHY J. HEALEY[3,4] & UĞUR ALYANAK[3]

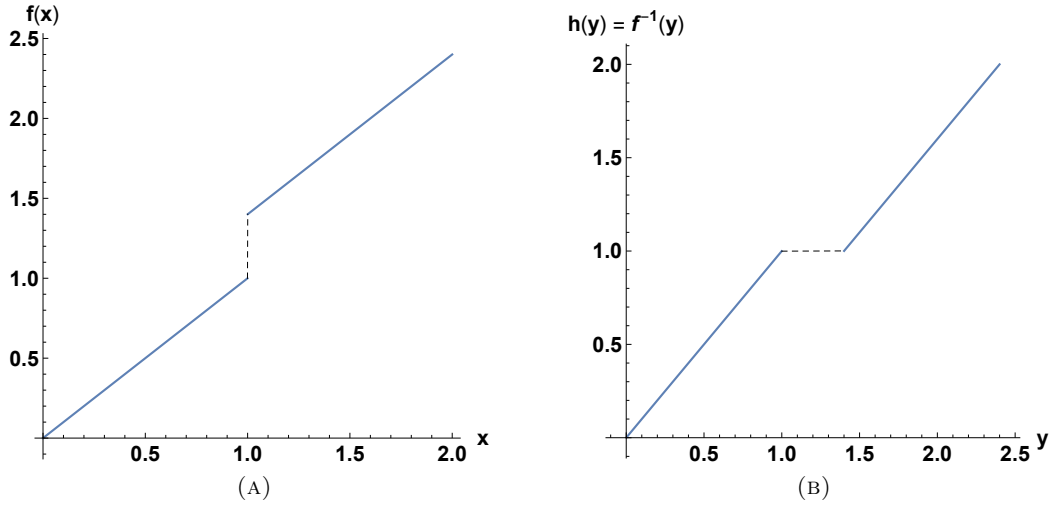
Abstract. We propose a one-dimensional, nonconvex elastic constitutive model with higher gradients that can predict spontaneous fracture at a critical load via a bifurcation analysis. It overcomes the problem of discontinuous deformations without additional field variables, such as damage or phase-field variables, and without *a priori* specified surface energy. Our main tool is the use of the inverse deformation, which can be extended to be a piecewise smooth mapping even when the original deformation has discontinuities describing cracks opening. We exploit this via the inverse-deformation formulation of finite elasticity due to Shield and Carlson, including higher gradients in the energy. The problem is amenable to a rigorous global bifurcation analysis in the presence of a unilateral constraint. Fracture under hard loading occurs on a bifurcating solution branch at a critical applied stretch level and fractured solutions are found to have surface energy arising from higher gradient effects.

1. Introduction

A major difficulty in modelling brittle fracture of solids is that cracks are usually represented via discontinuous deformations. Whereas discontinuous gradients of the deformation can be described by nonlinear elasticity, and can be regularized by higher gradient terms in the stored energy, it is not clear how to deal with discontinuities of the deformation in a similar way. To circumvent this issue, various ingenious fracture models have been developed that introduce the crack as a separate entity, *a priori* endowed with properties that are distinct from the constitutive law of the bulk material, such as surface energy, cohesive laws, damage variables or phase fields, e.g., [1, 2, 3, 4, 5, 6].

A distinctive approach is Truskinovsky's treatment of fracture as a phase transition [7], where fracture results from nonconvexity of a two-well stored energy function, with the transformation strain (location of the second well) going to infinity; it involves strains in the fracture zone that become unbounded in that limit. It would be desirable to regularize this nonconvex problem using higher gradients, but this leads to unbounded energies. So, while we embrace the idea of fracture as a phase change, the question remains how to model fracture in this spirit, somehow avoiding singularities and additional constitutive ingredients for the crack.

Here we introduce a local, elastic, nonconvex constitutive model that is amenable to regularization by higher gradients. It can predict fracture with the spontaneous appearance of discontinuous deformations via bifurcation of equilibria, but does not involve additional field variables, such as damage or phase-field variables, or an *a priori* specified surface energy for cracks. Our main tool is the inverse deformation, which can be extended to



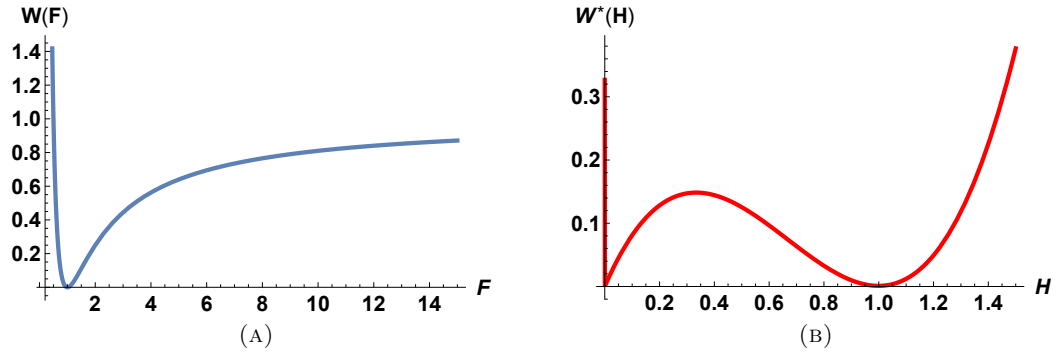
(A) (B)

FIGURE 1. (A) A cracked deformation (blue) with a vertical segment (black) attached to render the graph a continuous curve. (B) The generalized inverse of the cracked deformation. The horizontal segment (black) is the opened crack in the deformed configuration.

a be piecewise smooth mapping even when the original deformation has discontinuities describing crack opening. We exploit this through the inverse-deformation formulation of finite elasticity due to Shield [8].

Motivation. Our first observation concerns one-dimensional fractured deformations, viewed here as strictly monotone mappings that involve at least one jump discontinuity (a crack). The graph of such a function has disjoint pieces that can be joined together by vertical segments of "infinite slope" as in Fig. 1a. One can then easily construct a generalized inverse of this deformation by interchanging the abscissa and the ordinate. The graph of this inverse has strictly increasing pieces that are the graphs of the (standard) inverses of the deformation on either side of the crack. Moreover their graphs are connected by a horizontal segment, which corresponds to the "inverse" of the segment of infinite slope. The generalized inverse so constructed is a piecewise smooth mapping, where two or more "phases" of positive stretch are separated by one or more "phases" of zero stretch. To allow for the latter, we extend the notion of deformation to admit nonnegative, as opposed to strictly positive, derivatives, so that mere non-strict monotonicity is required.

In a sense, the inverse deformation closes the crack, as it maps each crack interval to a single point, the reference location of the crack. In Fig. 1, the interval $1 \leq y \leq 1.4$ is mapped back to the point $x = 1$. Analogously, the original deformation opens the crack (at $x = 1$ in the example), as it maps the single crack point in the reference configuration to the cracked interval in the deformed configuration ($1 \leq y \leq 1.4$ in the example, or the gap between the two opened-crack faces). A major advantage is that unlike the discontinuous original



(A) (B)

FIGURE 2. (A) A stored energy function of a material that undergoes brittle fracture (cf. (5.36) in Example 5.10). (B) The corresponding inverse stored energy function W^*.

deformation, the generalized inverse, Fig. 1b, is Lipschitz continuous and has gradient discontinuities, like a two-phase deformation [9]. Here, intervals of positive inverse stretch are separated by intervals of zero inverse stretch. These we identify with the uncracked phase and the cracked phase, respectively. The length of a cracked-phase interval is nothing but the crack opening displacement.

Another crucial advantage of the inverse description is that the analogy with phase transitions extends naturally to the constitutive law itself, once we invoke the inverse deformation approach of Shield [8], as we now explain. A material suffering brittle fracture in a one-dimensional setting is typically characterized by an elastic stored energy function of the form shown in Fig. 2b, having a convex well at the reference state, but eventually becoming concave and approaching a horizontal asymptote from below as the stretch tends to infinity. The inverse stored energy function W^* is related to the (usual) stored energy function W by [8]

$$W^*(H) = HW(1/H), \quad H > 0,$$

and has the property that the elastic energy of a deformation $f : [0,1] \to [0,\lambda]$ can be written as

$$\int_0^1 W(f'(x))dx = \int_0^\lambda W^*(h'(y))dy,$$

where $h = f^{-1}$ is the inverse deformation, and the *inverse stretch* is

$$H(y) = h'(y) = 1/f'(x), \quad \text{where } x = f^{-1}(y).$$

For W as in Fig. 2a, the inverse stored energy W^* would be as in Fig. 2b,, where we now extend its domain of definition as follows

$$W^*(H) = \begin{cases} HW(1/H), & H > 0 \\ 0, & H = 0 \\ \infty, & H < 0. \end{cases} \tag{1.1}$$

Here we allow the possibility that the inverse stretch $H = h' = 0$ (corresponding to the cracked phase as discussed above), but prohibit $h' < 0$, which corresponds to $f' < 0$, namely, orientation-reversing interpenetration. We recall that the case $h' = 0$ corresponds to crack opening, not interpenetration. Instead of the usual constraint $f' > 0$, we thus impose $h' \geq 0$ as a constraint. When one visualizes this unilateral constraint as a vertical barrier just to the left of 0 as part of the graph of W^* (Fig. 2b), it is clear that the latter has the form of a two-well energy, with wells at $H = 0$ and $H = 1$. The inverse deformation of Fig. 1b is a zero-energy one (global minimizer) provided that the rising portions have slope $H = 1$, since the flat portion has slope $H = 0$. In Fig. 2b, the well at $H = 1$ corresponds to the undeformed, uncracked "phase", while the well at $H = 0$ to the cracked "phase". The length of the interval in the $H = 0$ phase (horizontal segment in Fig. 2b) is the crack opening displacement. In this sense, the 0 phase is "thin air" or empty space between crack faces. To see this, consider local mass balance in terms of the inverse deformation, which reads

$$\rho_0 H = \rho, \tag{1.2}$$

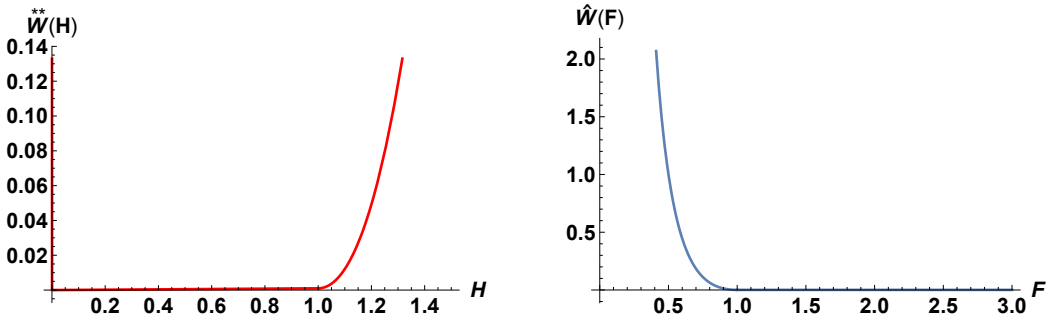
where $\rho_0 > 0$ is the reference density and ρ the deformed density. Clearly, for $H = 0$ this implies $\rho = 0$, absence of matter, or empty space. Our viewpoint is that fracture corresponds to two-phase inverse deformations minimizing this two-well energy, where intervals in the $H = 0$ phase are opened cracks in the deformed configuration.

A standard relaxation of this two-well energy gives the convexification $\overset{**}{W}$ of W^* (together with the constraint $h' \geq 0$). This corresponds to a material that cannot resist compression (Fig. 3a). Also $\overset{**}{W}$ is the inverse stored energy function of $\widehat{W}$, which has the form shown in Fig. 3b, corresponding to a material that cannot sustain tension. The drawback here is that minimizers h of the inverse energy can have an arbitrary number of cracked intervals $H = 0$ alternating with intervals where $H = 1$, corresponding to arbitrary positions of cracks in the reference configuration. Another problem is that this material breaks at the slightest pull.

To fix these problems, we exploit the final advantage of the inverse approach. The problem associated with W^* can be regularized by the addition of higher gradients of the inverse deformation h to the energy which would become

$$E_\varepsilon\{h\} = \int_0^\lambda W^*(h'(y))dy + \frac{\varepsilon}{2}\int_0^\lambda [h''(y)]^2 dy, \tag{1.3}$$

subject to the unilateral constraint $h' \geq 0$ on $[0, \lambda]$. The analogous attempt to add higher gradients of the original deformation f to the energy runs into difficulties because of the discontinuities of f (Fig. 1a); such deformations cannot be approximated by smooth functions and still maintain bounded energy, if higher-gradients are included in the usual way. A major strength of the inverse approach lies in the simplicity of the model energy (1.3) and the relative mathematical ease with which its equilibria are studied. Even though the original deformation is discontinuous, the inverse deformation can be extended to be Lipschitz. In fact, we show that equilibria of the second-gradient energy (1.3) are C^1, including



(A) (B)

FIGURE 3. (A) The convexification $\overset{**}{W}$ of W^* of Fig. 2b. (B) The stored energy function $\hat{W}$ whose inverse stored energy is $\overset{**}{W}$.

intervals of zero inverse stretch $h' = 0$, corresponding to opened cracks in the deformed configuration. In the presence of such intervals, the original deformation is discontinuous.

Methods. The inverse formulation of Shield & Carlson [8, 10], combined with inspiration from Truskinovsky's idea of fracture as a phase transition [7] , allows us to treat the problem as a constrained, but otherwise standard, two-well elasticity problem with higher gradients. We note that the model does not involve any special treatment for cracks, such as separate cohesive energies, different spatial scales for crack zones, "exotic" spaces such as SBV, or additional phase fields.This general approach is promising, and it begs the question of two or three dimensional formulations, which we pursue elsewhere [11].

We study equilibria of the displacement problem in the inverse formulation, taking $E_\varepsilon\{h\}$ in (1.3), to be the energy in terms of the inverse deformation h. We employ techniques of global bifurcation theory [12], keeping in mind that stable branches of local energy minima may occur, while exploiting phase plane techniques in the spirit of [13]. The only complication here is the unilateral constraint $h' \geq 0$ on the inverse deformation, in an otherwise fairly standard two-well problem with higher gradients like [13, 14, 6]. We formulate the problem as a variational inequality incorporating the constraint, and employ the methods of [15].

To obtain quantitative information on bifurcating solution branches, we choose specific examples of the stored-energy function W of the form shown in Fig. 1b, and either compute solutions using the bifurcation/continuation program AUTO [16], or obtain branches analytically or semi-analytically in some cases.

Results. The results are consistent with our expectations of one-dimensional brittle fracture, and agree with some predictions of discrete models [17]: In particular, pulling on a bar with prescribed end displacement deforms it homogeneously until the end displacement reaches a critical level. After that, the stress drops suddenly to zero and remains there during further elongation; the bar is broken See Fig. 4. On the end-load *vs* average-stretch

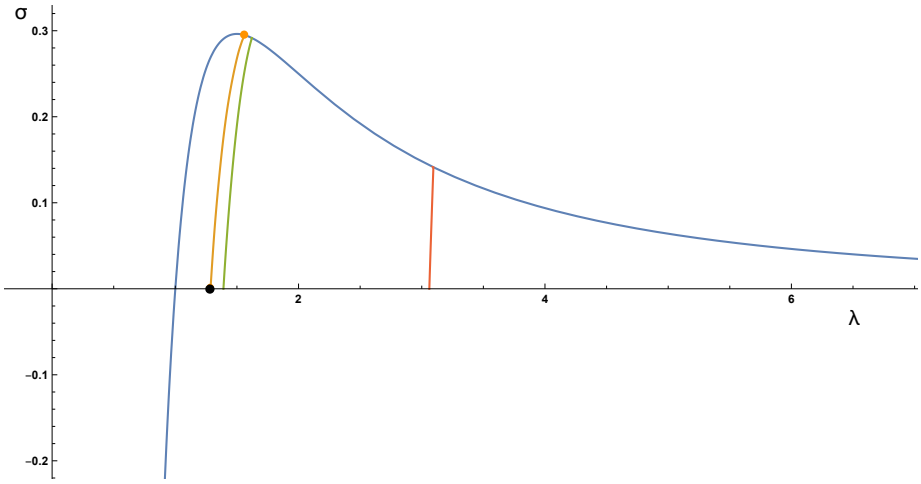


FIGURE 4. The trivial solution branch and first bifurcating branch for various values of ε, represented in the (σ, λ) or stress *vs* average-stretch plane (for the special constitutive law (5.36) in Example 5.10). Blue curve: trivial solution branch corresponding to homogeneous deformation. Orange, green and red curves, first bifurcating branch for different values of $\varepsilon = 2/49$, $2/25$ and 2, respectively. For example, if $\varepsilon = 2/49$, the trivial branch is stable to the left of the orange dot (1st bifurcation point) and unstable to the right. The horizontal axis to the right of the black dot (lowest point of the orange curve) consists of stable broken solutions. Similarly for the other cases.

diagram this corresponds to the portion of the blue curve to the left of the orange dot (for $\varepsilon = 2/49$). The blue curve corresponds to the trivial branch of solutions with uniform stretch. The orange dot is the first bifurcation point, just after the maximum of the stress-stretch curve for small ε. Beyond that the homogeneous stretch solution (blue curve) is unstable. The first nontrivial branch of bifurcating solutions (orange curve) eventually connects to the zero-stress axis at the black dot in Fig. 4. This point corresponds to initiation of fracture.

The first branch then continues along the horizontal zero-stress axis to the right of the black dot. The bar breaks at one of the two ends, and the stress vanishes thereafter, as the end displacement is further increased. Points on the horizontal axis to the right of the black dot in Fig. 4 correspond to broken solutions. The broken bar has vanishing stress and is virtually undeformed except for a transition layer, followed by a closed interval of zero inverse stretch, which corresponds to the opened crack. The length of this interval equals the crack opening displacement.

Broken solutions are endowed with additional surface energy, because of higher gradients. To leading order in the higher gradient coefficient ε, this surface energy is determined

explicitly given the stored energy function:

$$\text{Surface Energy} = \sqrt{\varepsilon}\int_0^1 \sqrt{2W^*(H)}dH = \sqrt{\varepsilon}\int_1^\infty \sqrt{2W(F)/F^5}dF.$$

It plays a role similar to the one posited by Griffith.

The inverse deformation is smooth, but the original deformation is discontinuous at the broken end. All solutions with more than one fracture are unstable; they arise from higher-mode branches bifurcating off the homogeneous solution, that are all unstable.

Longer bars are more brittle (break sooner and more suddenly) than shorter bars. This is because rescaling shows that the energy (1.3) of a bar of reference length L and higher gradient coefficient ε is equal to the energy of a bar of unit reference length and a higher gradient coefficient $\bar{\varepsilon} = \varepsilon/L^2$, while the fracture stretch increases with ε. In particular, very short bars, or nanoparticles, are stable in uniform stretch well beyond the maximum of the stress-stretch curve, as observed by Gao [18].

Some of our predictions differ from the results of some other models. First, the crack faces are sharply defined points, and the crack is empty of matter, in contrast to damage or phase field models, e.g., [5], where the crack is diffuse. This occurs despite the smoothening effect of higher gradients, and is related to the unilateral constraint $h' \geq 0$. Second, upon fracture, the stress suddenly drops suddenly to zero at a finite macroscopic stretch, and stays zero thereafter, instead of approaching zero for large elongation, which occurs in some cohesive-zone and nonlocal models, e.g., [19, 6]. This agrees with the common concept of brittleness. We note that the stress-stretch constitutive relation underlying our model only asymptotically approaches zero as the stretch goes to infinity. The sudden drop to zero stress at finite applied stretch is a consequence of material instability and bifurcation to an inhomogeneous state. Finally, our formulation and results are relevant to large deformations, the only setting in which the inverse-deformation approach makes sense.

We now give an outline of the work. In Section 2 we consider the inverse-stretch formulation, presuming hard loading in the presence of both an integral constraint (for compatibility with imposed end displacements) and the unilateral constraint of nonnegative inverse stretch. We demonstrate the existence of a global energy minimizer, and proceed to formulate the Euler-Lagrange variational inequality governing all equilibria. We reformulate the variational inequality accounting for the integral constraint and demonstrate that all equilibria are C^1. We end the section with some *a priori* bounds. In Section 3 we prove the existence of global solution branches bifurcating from the trivial, homogeneous solution. We employ methods of global bifurcation for variational inequalities [15] to obtain branches of nontrivial (non-homogeneous) solutions via the methodology of [12], and we establish nodal properties of solutions as in [20]. The latter, combined with the *a priori* bounds, imply that all bifurcating branches of equilibria are unbounded. In Section 4 we obtain more detailed properties of solutions via qualitative phase-plane arguments. In particular, we show that each global solution branch has a bounded component that connects the bifurcation point to another solution exhibiting the onset of fracture, marked by vanishing of the inverse stretch at some point. The *a priori* bounds of Section 2 play a

key role here. Our qualitative analysis also reveals the structure of all further broken solutions on the complementary, unbounded component of the solution branch. These broken solutions are characterized by the presence of nonempty, closed intervals of zero inverse stretch. We finish the section with some stability results. We demonstrate that the trivial solution is locally stable up to the first bifurcation point, and unstable beyond it, and we show that all bifurcating solutions of mode higher than 1 are also unstable. In Section 5 we convert our results, *a posteriori*, to the original Lagrangian variables. In particular, we obtain the effective end-load *vs* average stretch curve as in [14] via projection of the first global solution branch. Here the homogeneous solution appears as the nominal constitutive law (stress-stretch relation). For large enough average stretch, we observe that the only possibility for an energy minimizer (under hard loading) is the broken solution along the first bifurcating branch. We finish the section with a semi-analytical characterization of the first branch and the fracture stretch, and some concrete results for specific models—some analytical and some numerical.

2. Formulation and A Priori Estimates

We start with assumptions for W that are typical of one-dimensional brittle fracture and in accordance with the properties suggested in Fig. 2:

$$\begin{array}{l} W\in C^3(0,\infty);\ \ W(F)\nearrow\infty\ \text{ as }\ F\searrow 0;\ \ W(F)\nearrow\gamma>0\ \text{ as }\ F\nearrow\infty;\\ W(1)=0;\ \ W(F)>0,\ \ F\neq 1;\\ W\ \text{ is strictly convex on } [0,1/\kappa) \text{ and strictly concave on } (1/\kappa,\infty),\ \text{ where }\ \ 0<\kappa<1. \end{array} \tag{2.1}$$

As a consequence of (1.1), and letting $\dot{W}^*(H)=dW^*(H)/dH$, it follows that

$$\begin{array}{l} W^*\in C^3(0,\infty);\ \ W^*(0)=W^*(1)=0;\ \ W^*(H)>0,\ \ H\neq 0,1;\ \ \dot{W}^*(0^+)=\gamma;\\ W^*\ \text{ is strictly concave on } [0,\kappa) \text{ and strictly convex on } (\kappa,\infty). \end{array} \tag{2.2}$$

We write the total potential energy (1.3) in terms of the inverse stretch $H=h'$ (derivative of the inverse deformation h):

$$E_\varepsilon[H]=\int_0^\lambda [\frac{\varepsilon}{2}(H')^2+W^*(H)]dy, \tag{2.3}$$

with $\varepsilon,\lambda>0$. We consider "hard" loading, namely Dirichlet boundary conditions on the original deformation $f(0)=0,\ \ f(1)=\lambda$. Here $\lambda>0$ is the prescribed deformed length of the bar, whose reference length equals unity. As a result, the inverse deformation is subject to $h(0)=0,\ \ h(\lambda)=1$. The inverse stretch is thus subject to two constraints

$$\int_0^\lambda H(y)dy=1,\qquad H\geq 0\ \text{ on }\ [0,\lambda], \tag{2.4}$$

for $\lambda\in(0,\infty)$. The second above allows for $H=0$, which, as discussed in the Introduction, corresponds to crack opening. For convenience, we change variables as follows:

$$y=\lambda s,\ \ 0\leq s\leq 1;\qquad u(s):=\lambda H(\lambda s)-1. \tag{2.5}$$

Then (2.3), (2.4) are equivalent to

$$V_\varepsilon[\lambda, u] = \int_0^1 [\frac{\varepsilon}{2}(u')^2 + \lambda^4 W^*([1+u]/\lambda)]ds, \tag{2.6}$$

subject to

$$\int_0^1 u(s)ds = 0; \qquad u \geq -1 \text{ on } [0,1], \tag{2.7}$$

respectively.

We define the Hilbert space

$$\mathcal{H} := \{v \in H^1(0,1) : \int_0^1 v ds = 0\}, \tag{2.8}$$

with inner product

$$\langle u, v\rangle := \int_0^1 u'v' ds, \tag{2.9}$$

along with the admissible set

$$\mathcal{K} := \{v \in \mathcal{H} : v \geq -1 \text{ on } [0,1]\}, \tag{2.10}$$

which is closed and convex. We remark that the inner product (2.9) on $\mathcal{H}$ is equivalent to the usual $H^1(0,1)$ inner product, by virtue of a Poincare inequality.

Since the integrand in (2.6) is quadratic and convex in the argument u', the following is standard:

Proposition 2.1. *$u \mapsto V_\varepsilon[\lambda, u]$ attains its minimum on $\mathcal{K}$ for each $\lambda \in (0,\infty)$.*

Proof. Clearly $V_\varepsilon[\lambda, \cdot]$ is coercive and sequentially weakly lower semi-continuous on $\mathcal{H}$. Let $\{u_k\} \subset \mathcal{K}$ be a minimizing sequence. Then for a subsequence, $u_{k_j} \rightharpoonup u$ weakly in $\mathcal{H}$, and by compact embedding, $u_{k_j} \to u$ uniformly on $[0,1]$. Since each $u_{k_j} \geq -1$ on $[0,1]$, it follows that $u \in \mathcal{K}$. □

Now let $u, v \in \mathcal{K}$, and consider $e(t) := E[(1-t)u + tv]$, $t \in [0,1]$. Then u is a critical point (equilibrium) if $e'(0) \geq 0$, which yields the (Euler-Lagrange) variational inequality

$$\int_0^1 [\varepsilon u'(v-u)' + \lambda^3 \dot{W}^*([1+u]/\lambda)(v-u)]dx \geq 0 \text{ for all } v \in \mathcal{K}, \tag{2.11}$$

where $\dot{W}^*(H) := \frac{d}{dH}W(H)$. We establish some general properties of solutions of (2.11), postponing for now the construction of other equilibria beyond global energy minimizers. Define the interior

$$\mathcal{K}^o := \{u \in \mathcal{K} : u > -1 \text{ on } [0,1]\}, \tag{2.12}$$

and suppose that $u \in \mathcal{K}^o$ satisfies (2.11). Let $\psi, \varphi \in H^1(0,1)$ such that $\int_0^1 \varphi dx = 1$, and set $h = \psi - \varphi \int_0^1 \psi dx$. Then $h \in \mathcal{H}$, and $v = u \pm th \in \mathcal{K}$, for $t > 0$ sufficiently small. Employing these two test functions in (2.11), we conclude that

$$\int_0^1 [\varepsilon u'\psi' + \{\lambda^3 \dot{W}^*([1+u]/\lambda) - \mu\}\psi]ds = 0 \text{ for all } \psi \in H^1(0,1), \tag{2.13}$$

where μ is a constant (Lagrange) multiplier. This leads to:

Proposition 2.2. *An interior point $u \in \mathcal{K}^o$ is a solution of (2.11) for $\lambda \in (0,\infty)$, if and only if $u \in C^2[0,1]$ satisfies*

$$\begin{array}{l} -\varepsilon u'' + \lambda^3 \dot{W}^*\left([1+u]/\lambda\right) = \lambda^3 \int_0^1 \dot{W}^*\left([1+u(\tau)]/\lambda\right) d\tau, \;\; 0<x<1; \\ u'(0) = u'(1) = 0; \qquad \int_0^1 u ds = 0. \end{array} \tag{2.14}$$

Proof. If $u \in \mathcal{K}^o$ satisfies (2.11) then (2.13) holds, and by embedding, $u \in C[0,1]$. Thus, (2.13) implies directly that the second distributional derivative of u can be identified with a continuous function. An integration by parts in (2.13) then delivers

$$\varepsilon u'' = \lambda^3 \dot{W}^*([1+u]/\lambda) - \mu, \;\; 0<x<1, \tag{2.15}$$

as well as the boundary conditions $(2.14)_2$. The nonlocal form $(2.14)_1$ follows by integrating (2.15) over $(0,1)$ while making use of the boundary conditions. The integral constraint $(2.14)_3$ is automatic, cf. (2.8). Finally, (2.15) along with $u \in C[0,1]$ imply that u is C^2 on the closed interval. The converse statement is obvious; starting with (2.14), the above steps are reversible. □

Next, for given solution pair $(\lambda, u) \in (0,\infty) \times \mathcal{K}$ of (2.11), we define the closed *broken set*

$$\mathcal{B}_u := \{s \in [0,1] : u(s) = -1\}, \tag{2.16}$$

and the open *glued set*

$$\mathcal{G}_u := \{s \in [0,1] : u(s) > -1\}. \tag{2.17}$$

Clearly $\mathcal{G}_u \cup \mathcal{B}_u = [0,1]$, and in view of (2.7), we note that $\mathcal{G}_u \neq \emptyset$.

Theorem 2.3. *Any solution $u \in \mathcal{K}, \lambda \in (0,\infty)$, of (2.11) is continuously differentiable on $[0,1]$. Moreover, $u \in C^2(\mathcal{G}_u)$.*

Proof. We choose $\psi, \varphi \in H^1(0,1)$ as before leading to (2.13), except we also require here that $\psi \geq 0$ and $h \geq 0$ on $\mathcal{B}_u$. Setting $v = u + h \in \mathcal{H}$ in (2.11) then leads to

$$\int_0^1 [\varepsilon u'\psi' + \{\lambda^3 \dot{W}^*\left([1+u]/\lambda\right) - \mu\}\psi] ds \geq 0 \;\text{ for all }\; \psi \in H^1(0,1) \;\text{ with }\; \psi \geq 0 \;\text{ on }\; \mathcal{B}_u, \tag{2.18}$$

where μ is a constant multiplier. Specializing (2.18) to test functions ψ vanishing on $\mathcal{B}_u$, we obtain

$$\int_{\mathcal{G}_u} [\varepsilon u'\psi' + \{\lambda^3 \dot{W}^*\left([1+u]/\lambda\right) - \mu\}\psi] ds = 0 \quad \text{for all } \psi \in H^1(0,1) \text{ with } \psi = 0 \text{ on } \mathcal{B}_u. \tag{2.19}$$

The same arguments used in the proof of Proposition 2.2 now show that $u \in C^2(\mathcal{G}_u)$ satisfies the differential equation

$$\varepsilon u'' = \lambda^3 \dot{W}^*([1+u]/\lambda) - \mu \text{ in } \mathcal{G}_u. \tag{2.20}$$

A version of the Riesz representation theorem implies that the left side (2.18) is characterized by a non-negative Radon measure $\mathfrak{m}$, which in view of (2.20), has support in $\mathcal{B}_u$, viz.,

$$\int_0^1 [\varepsilon u'\psi' + \{\lambda^3 \dot{W}^*([1+u]/\lambda) - \mu\}\psi]ds = \int_{\mathcal{B}_u} \psi d\mathfrak{m}(s) \text{ for all } \psi \in H^1(0,1). \tag{2.21}$$

Arguing as in [21], we set $\varphi(s) := \mathfrak{m}([0,s))$, which is non-decreasing. Then (2.21) implies

$$\varepsilon u'(s) = \lambda^3 \int_0^s \dot{W}^*([1+u(\xi)]/\lambda)d\xi - \mu s - \varphi(s) + C, \tag{2.22}$$

where C is a constant. Since φ is non-decreasing, (2.22) shows that $u'(s^+) \le u'(s^-)$ on $[0,1]$. Now consider $s \in \mathcal{B}_u$, i.e., $u(s) = -1$, and thus $u(t) - u(s) \ge -1 - (-1) = 0$. Examination of the difference quotient $[u(t) - u(s)]/(t-s)(t \ne s)$ in the limit from the right and from the left as $t \to s$ reveals that $u'(s^+) \ge 0 \ge u'(s^-)$. □

Remark 2.4. *An energy minimizer, say, $u_\lambda, \lambda \in (0,\infty)$, given by Proposition 2.1, always satisfies* (2.11)*. As such, $u_\lambda \in C^1[0,1]$, by virtue of Theorem 2.3.*

Given that any solution u of (2.11) is C^1 with $u \equiv -1$ on $\partial\mathcal{G}_u$, integration of (2.20) as in the proof of Proposition 2.2 yields

Corollary 2.5. *Given a solution pair (λ, u) as in Theorem 2.3, then for any $(a,b) \subset \mathcal{G}_u$ with $a, b \in \partial\mathcal{G}_u$,*

$$\begin{gathered} -\varepsilon u'' + \lambda^3 \dot{W}^*([1+u]/\lambda) = \tfrac{\lambda^3}{b-a}\textstyle\int_a^b \dot{W}^*([1+u(\tau)]/\lambda)d\tau \text{ in } \mathcal{G}_u, \\ u'(a) = u'(b) = 0, \end{gathered} \tag{2.23}$$

and u is C^2 on $[a,b]$. If $[0,b) \subset \mathcal{G}_u$ with $b \in \partial\mathcal{G}_u$, then (2.23) *holds with $a = 0$. Likewise if $(a,1] \subset \mathcal{G}_u$ with $a \in \partial\mathcal{G}_u$, then* (2.23) *holds with $b = 1$.*

Next, we obtain bounds on nontrivial solutions $u \ne 0, \lambda \in (0,1)$. Define $M > 1$ via $\dot{W}^*(M) = \gamma := \dot{W}^*(0)$, cf. Fig. 5a.

Theorem 2.6. *Any nontrivial solution pair of* (2.11)*, $(\lambda, u) \in (0,\infty) \times \mathcal{K}$, $u \ne 0$, is characterized by*

$$\begin{gathered} \lambda > 1/M, \\ \|u\|_\infty \le C_\lambda, \quad \|u\|_{C^1} = \|u\|_\infty + \|u'\|_\infty \le C_{\lambda,\varepsilon}, \end{gathered} \tag{2.24}$$

where $\|\cdot\|_\infty$ denotes the maximum norm over $[0,1]$, and $C_\lambda, C_{\lambda,\varepsilon}$ are constants having dependence upon the indicated subscripted quantities, but independent of u.

Proof. Given that $u \ge -1$ is automatic, with $u \equiv -1$ on $\mathcal{B}_u$, we only require upper bounds on nontrivial solutions $u \in \mathcal{G}_u$. In view of Corollary 2.5, we consider any $(a,b) \subset \mathcal{G}_u$ with $a, b \in \partial\mathcal{G}_u$, or $[0,b) \subset \mathcal{G}_u$ with $b \in \partial\mathcal{G}_u$, or $(a,1] \subset \mathcal{G}_u$ with $a \in \partial\mathcal{G}_u$. Since u attains both its maximum and its minimum somewhere on the appropriate closed interval, there are points s_m, s_M such that

$$\begin{gathered} \max u(s) = u(s_M), \quad \min u(s) = u(s_m), \\ \text{with} \quad u(s_m) < 0 < u(s_M), \\ u''(s_m) \ge 0 \text{ and } u''(s_M) \le 0, \end{gathered} \tag{2.25}$$

where $(2.25)_2$ is a consequence of $(2.7)_1$. If s_m and/or s_M are boundary points, then $(2.25)_3$ are one-sided derivatives, as justified in Corollary 2.5. We now evaluate (2.23) at s_m and at s_M, respectively, subtract the resulting equations and employ $(2.25)_3$ to deduce

$$\dot{W}^*([1+u(s_M)]/\lambda) \leq \dot{W}^*([1+u(s_m)]/\lambda). \tag{2.26}$$

From the graph of $\dot{W}^*(\cdot)$, cf. Fig. 5, it follows that both $(2.25)_2$ and (2.26) can be fulfilled only if

$$0 < 1/\lambda \leq M \ \text{ and } \ 0 \leq [1+u(s_m)]/\lambda < [1+u(s_M)]/\lambda \leq M, \tag{2.27}$$

which is equivalent to

$$\lambda \geq 1/M \ \text{ and } -1 \leq u(s_m) < u(s_M) \leq -1+\lambda M \tag{2.28}$$

This yields $(2.24)_{1,2}$, with $C_\lambda := \max\{1, -1+\lambda M\}$. Combining (2.28) with $(2.23)_1$ (bootstrap) yields $(2.24)_3$. □

Corollary 2.7. *$0 \leq H(y) < M$ for all $y \in [0,\lambda]$.*

3. Equilibria via Global Bifurcation

In this section we consider the existence of other critical points via bifurcation from the trivial solution. In particular, note that $0 \in \mathcal{K}^o$, and thus, according to Proposition 2.2, the trivial solution branch $u \equiv 0$ for all $\lambda \in (0,\infty)$, satisfies (2.14). To begin, we consider the formal linearization of (2.14) at $u = 0$:

$$\begin{aligned} &-\varepsilon h''(s) + \lambda^2 \ddot{W}^*(1/\lambda) h(s) = 0, \quad 0 < s < 1, \\ &h'(0) = h'(1) = 0, \ \ \textstyle\int_0^1 h(s)ds = 0, \end{aligned} \tag{3.1}$$

where $\ddot{W}^* := \frac{d^2 W^*}{dH^2}$. Clearly (3.1) admits nontrivial solutions

$$h(s) = h_n(s) := \cos(n\pi s), \ \ n = 1, 2, \ldots, \tag{3.2}$$

provided that the characteristic equation

$$\frac{\varepsilon n^2 \pi^2}{\lambda^2} = -\ddot{W}^*(1/\lambda), \tag{3.3}$$

has corresponding roots λ_n, $n = 1, 2, \ldots$ For each value of $n \in \mathbb{N}$, the left side of (3.3) defines a parabola in the variable $1/\lambda$. Then taking into account the graph of $-\ddot{W}^*(\cdot)$, cf. (2.2) and Fig. 5b, we conclude that (3.3) has a countable infinity of simple transversal roots:

$$1/\kappa < \lambda_1 < \lambda_2 < \ldots, \tag{3.4}$$

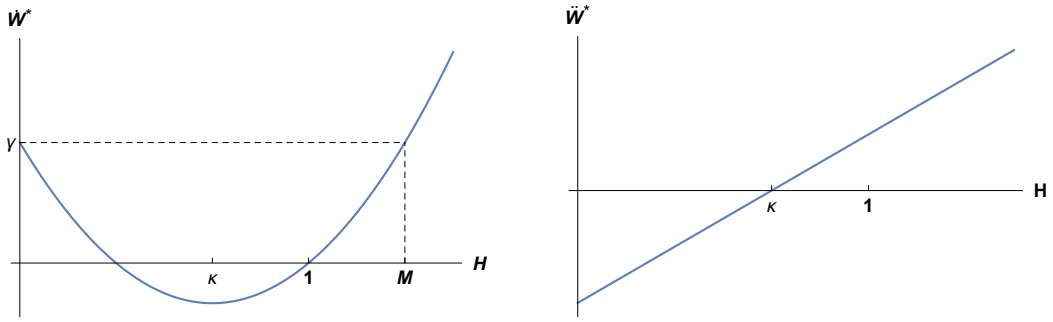
each of which corresponds to a respective nontrivial solution (3.2).

To carry out a rigorous bifurcation analysis, we follow the approach in [15]. We first express (2.11) abstractly via

$$\langle \varepsilon u + G(\lambda, u), v - u \rangle \geq 0, \ \text{ for all } \ v \in K, \tag{3.5}$$

with $G : (0,\infty) \times \mathcal{H} \to \mathcal{H}$ defined by

$$\langle G(\lambda, u), v \rangle := \lambda^3 \int_0^1 \dot{W}^* \left([1+u(x)]/\lambda\right) v(s) ds, \tag{3.6}$$



(A) (B)

FIGURE 5. (A) $\dot{W}^*$ *vs* H. (B) $\ddot{W}^*$ *vs* H .

for all $v \in \mathcal{H}, \lambda \in (0,\infty)$. Observe that $\langle G(\lambda,0), v\rangle \equiv 0$ for all $v \in \mathcal{H}, \lambda \in (0,\infty)$. Since $\dot{W}^*$ is continuous, the compact embedding $H^1(0,1) \to C[0,1]$ implies that G is continuous and compact. Let $P_{\mathcal{K}}$ denote the closest-point projection of $\mathcal{H}$ onto $\mathcal{K}$, i.e., for any $f \in \mathcal{H}$, $\quad u = P_{\mathcal{K}} f \Leftrightarrow u \in \mathcal{K}$ and $\langle u - f, v - u\rangle \geq 0$ for all $v \in \mathcal{K}$. Then (3.5) is equivalent to the operator equation

$$\varepsilon u + F(\lambda, u) = 0, \tag{3.7}$$

where $F := P_{\mathcal{K}} \circ G$. Due to the continuity of the projection $P_{\mathcal{K}}$, it follows that F is continuous and compact on $\mathbb{R} \times \mathcal{K}$. Thus, the Leray-Schauder degree of $u \mapsto u + \varepsilon^{-1} F(\lambda, u)$ is well-defined.

Clearly $F(\lambda, 0) \equiv 0$, and $u \mapsto F \equiv G$ in a neighborhood of $0 \in \mathcal{K}^o$. By embedding, it follows that $u \mapsto G(\lambda, u)$ is differentiable on that same neighborhood, with Fréchet derivative $A(\lambda)h := D_u G(\lambda, 0)h = \lambda^2 \ddot{W}^*(1/\lambda)h$ for all $h \in \mathcal{H}$. Hence, the rigorous linearization of (3.7) at the trivial solution reads

$$\langle \varepsilon h + A(\lambda)h, v\rangle = 0 \ \text{ for all } \ h, v \in \mathcal{H}, \tag{3.8}$$

and an integration by parts shows that (3.8) is equivalent to the formal linearization (3.1). In particular, (3.2)-(3.4) imply that $(\lambda_n, 0) \in (0,\infty) \times \mathcal{K}^o$, $n = 1, 2, \ldots$, are potential bifurcation points of (3.7).

We observe that $A(\lambda) : \mathcal{H} \to \mathcal{H}$ is compact. Also, for all $\lambda \neq \lambda_n$ and $n = 1, 2, \ldots$, $u = 0$ is the only solution of (3.7) on $B_r(0) \subset \mathcal{H}$, denoting some sufficiently small ball of radius $r > 0$ centered at the origin. Accordingly, the Leray-Schauder linearization principle shows that the topological degree of $u \mapsto u + \varepsilon^{-1} F(\lambda, u)$ on $B_r(0) \subset \mathcal{H}$ is given by

$$\deg(I + \varepsilon^{-1} F(\lambda, \cdot), B_r(0), 0) = (-1)^{m(\lambda)}, \tag{3.9}$$

where $m(\lambda)$ denotes the number of negative eigenvalues, counted by algebraic multiplicity, of the linear operator $I + \varepsilon^{-1} A(\lambda)$, for $\lambda \in \{\lambda \in (0,\infty) : \lambda \neq \lambda_n, \ n = 1, 2, \ldots\}$. We can now state a global bifurcation existence result, cf. [12]:

Theorem 3.1. *Let $\mathcal{S} \subset (0,\infty) \times K$ denote the closure of all nontrivial solution pairs (λ, u) $(u \neq 0)$ of (3.7), and let $\mathcal{C}_n$ denote the connected component of $\mathcal{S}$ containing $(\lambda_n, 0)$. Then $(\lambda_n, 0), n = 1, 2, \ldots$, is a point of global bifurcation, viz., each solution branch $\mathcal{C}_n$ is characterized by at least one of the following:*

(i) $\mathcal{C}_n$ is unbounded in $(0,\infty) \times \mathcal{H}$,

(ii) $\{(\lambda_k, 0)\} \subset \mathcal{C}_n$, $k \neq n$.

Proof. We first observe that $(2.24)_1$ implies $\mathcal{C}_n \subset (1/M, \infty) \times \mathcal{K}$. So it is enough to demonstrate that $\deg(I + \varepsilon^{-1}F(\lambda_-, \cdot), B_r(0), 0) \neq \deg(I + \varepsilon^{-1}F(\lambda_+, \cdot), B_r(0), 0)$, for some $\lambda_- \in (\lambda_n - \delta, \lambda_n)$ and $\lambda_+ \in (\lambda_n, \lambda_n + \delta)$, for each $n = 1, 2, \ldots$, where $\delta > 0$ is sufficiently small. This is indeed the case here; the transversality of the roots (3.4) of (3.3) insures that $m(\lambda_+) = m(\lambda_-) + 1$ for each $n = 1, 2, \ldots$. Thus, the desired conclusion follows from (3.9). □

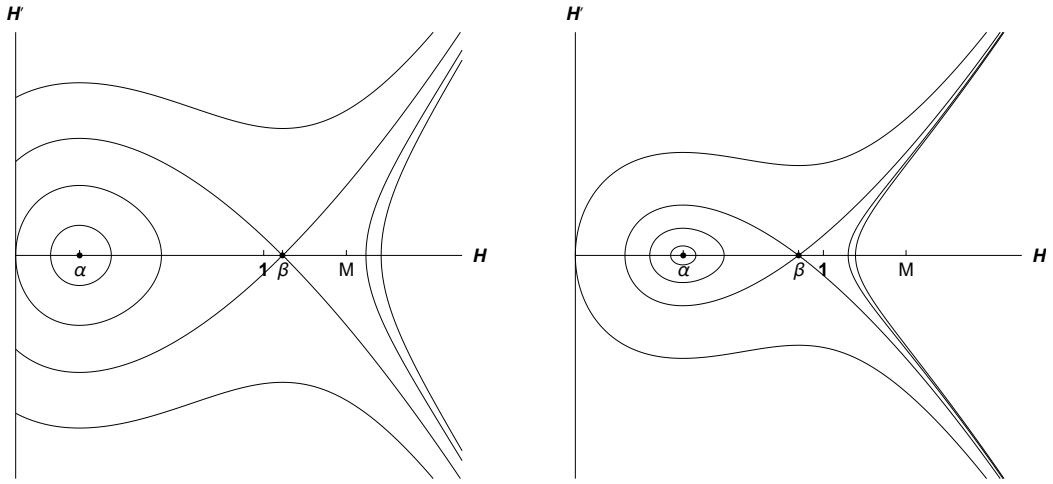
By virtue of embedding, each solution branch $\mathcal{C}_n \subset (0,\infty) \times \mathcal{H}$, $n = 1, 2, \ldots$, forms a continuum in $(0,\infty) \times C[0,1]$, and for any $(\lambda, u) \in \mathcal{C}_n$, we have that $u \in C^1[0,1]$, cf. Theorem 2.3. With that in hand, we now demonstrate that each branch is characterized by distinct nodal properties, generalizing a well-known result to our setting, cf. [20, 12]. Let $\mathcal{O}_\ell$ denote the open set of all functions $v \in C^1[0,1]$ having precisely ℓ zeros in $(0,1)$, each of which is simple, with $v(0) \neq 0$ and $v(1) \neq 0$. Let $\mathcal{C}_n^o$ denote the component of $\mathcal{C}_n \cap (0,\infty) \times \mathcal{K}^o$ containing the bifurcation point $(\lambda_n, 0)$, $\quad n = 1, 2, \ldots$ We call $\mathcal{C}_n^o \subset \mathcal{C}_n$ a sub-branch. The argument given in [20, 12] shows that nodal properties of solutions on global branches of 2^{nd} -order ODE such as (2.14) are inherited from the corresponding eigenfunction (3.2) and can change only at the trivial solution. As such, $\mathcal{C}_n^o \backslash \{(\lambda_n, 0)\} \subset (0,\infty) \times \mathcal{O}_n$, $n = 1, 2, \ldots$ In fact, this property holds for each of the global solution branches.

Proposition 3.2. *Each of the global bifurcating branches $\mathcal{C}_n$ of Theorem 3.1, is characterized by a distinct nodal pattern, viz.,*

$$\mathcal{C}_n \backslash \{(\lambda_n, 0)\} \subset (0,\infty) \times \mathcal{O}_n, \quad n = 1, 2, \ldots \tag{3.10}$$

As such, $\mathcal{C}_n \cap \mathcal{C}_m = \emptyset$, for all $m \neq n$, (alternative (ii) of Theorem 3.1 is not possible) and each $\mathcal{C}_n, n = 1, 2, \ldots$, is unbounded in $\mathbb{R} \times \mathcal{H}$.

Proof. Suppose that (3.10) does not hold. Given that $\mathcal{C}_n^o \backslash \{(0, \lambda_n)\} \subset (0,\infty) \times \mathcal{O}_n$, $n = 1, 2, \ldots$, it follows that there exists a nontrivial solution pair $(\lambda, u) \in \mathcal{C}_n \backslash \mathcal{C}_n^o$ with $u \in \partial\mathcal{O}_n$. This means there is some $x_o \in \mathcal{G}_u$ such that $u(x_o) = u'(x_o) = 0$. But then by the uniqueness theorem for (2.14), it follows that $u \equiv 0$ on $[a, b] \subset \overline{\mathcal{G}_u}$ for all such $(a, b) \subset \mathcal{G}_u$ with $a, b \in \partial\mathcal{G}_u$, or on $[0, b]$ with $b \in \partial\mathcal{G}_u$, or on $[a, 1]$ with $a \in \partial\mathcal{G}_u$. Theorem 2.3 together with $(2.7)_1$ then imply that $u \equiv 0$ on $[0, 1]$, i.e., nodal properties change only at the trivial solution. Finally, (3.10) along with the observation that $\mathcal{O}_n \cap \mathcal{O}_m = \emptyset$, for all $m \neq n$, imply that $\mathcal{C}_n \cap \mathcal{C}_m = \emptyset$, for all $m \neq n$, and hence, alternative (ii) of Theorem 3.1 is not possible. □



(A) (B)

FIGURE 6. Phase portraits for (4.3): (A) $\dot{W}^*(\kappa) < \varpi \leq 0$ (B) $0 < \varpi < \gamma$

4. Fracture and Stability

We consider fractured solutions, which involve a nonempty broken set (2.16), or at least one point $y \in [0,1]$ where $H(y) = 0$. The onset of fracture occurs when the broken set consists of isolated points. From such solutions, we construct others where the broken set consists of one or more intervals, e.g., (4.8) below, where necessarily the inverse deformation is constant, and the associated original deformation is discontinuous with opened cracks.

We demonstrate that fracture occurs on each of the bifurcating solution branches, and then obtain stability/instability results for some fractured solutions. We find it convenient to return to the original variables via (2.5), in which case the equilibrium equation (2.23) reads

$$\begin{aligned} -\varepsilon H'' + \dot{W}^*(H) = \varpi := \tfrac{1}{\lambda_*}\textstyle\int_{a_*}^{b_*} \dot{W}^*(H(\tau))d\tau \ \text{ on } \ (a_*, b_*), \\ H'(a_*) = H'(b_*) = 0, \end{aligned} \tag{4.1}$$

where $a_* := \lambda a$, $b_* := \lambda b$ and $\lambda_* := b_* - a_*$. Clearly any solution of (2.23) gives a solution of (4.1), and vice-versa.

In order to glean more information, we identify $(4.1)_1$ with a dynamical system, treating the independent variable "y" as a time-like. The critical points or "equilibria" correspond to solutions of the algebraic equation

$$\dot{W}^*(H) - \varpi = 0. \tag{4.2}$$

The graph of $\dot{W}^*$ reveals that when $\dot{W}^*(\kappa) < \varpi \leq \gamma := \dot{W}^*(0)$, there are two solutions of (4.2), denoted $H \equiv \alpha$, and $H \equiv \beta$, where $0 \leq \alpha < \beta \leq M$. cf. Fig. 5a. In addition, $(4.1)_1$ admits the first integral

$$\frac{\varepsilon}{2}(H')^2 - [W^*(H) - \varpi H] = \Gamma, \tag{4.3}$$

where Γ is a constant. With (4.3) in hand, we obtain the phase portraits depicted in Fig. 6, where α is a "center", and β is a "saddle". According to the boundary conditions $(4.1)_2$, the trajectories should "start and stop" on the H- axis. As such, we are interested only in closed orbits about the center

$$\alpha = 1/\lambda, \tag{4.4}$$

such that $H \geq 0$, cf. $(2.4)_2$. The right side of (4.4) follows from (2.5), given that the former represents the trivial solution, viz., $H \equiv 1/\lambda \;\; \Leftrightarrow u \equiv 0$.

Remark 4.1. *In view of* (4.4) *and Fig. 6, it follows that* $\lambda > 1$ *for non-negative solutions* $H \geq 0$*, which improves* $(2.28)_1$*. Referring again to* (4.2)*, the cases* $\varpi \leq \dot{W}^*(\kappa)$ *and* $\varpi > \gamma$ *are not associated with solutions of* (4.1)*. The first leads to either one degenerate critical point* $\alpha = \beta$ *(for* $\varpi = \dot{W}^*(\kappa)$*) or no critical points, while the second case yields only one (positive) critical point.*

According to Proposition 2.2, we infer that $(a_*, b_*) = (0, \lambda)$ in (4.1) for any strictly positive, non-constant solution $H > 0$, i.e., for $u \in \mathcal{K}^o, \;\; u > -1$, cf. (2.5). Moreover, we must choose only those phase curves yielding even, functions of period $2\lambda/\ell$, where ℓ is a positive integer. The first integral (4.3) implies that a non-constant, positive solution H of (4.1) of period $2\lambda/\ell$ has either a maximum at $y = 0$ and a minimum at $y = \lambda/\ell$, or vice-versa. In addition, H is strictly monotone on $(0, \lambda/\ell)$ and possesses reflection symmetry at the maximum and minimum locations, cf. [22]. In view of (2.5), these same qualitative properties hold for nontrivial solutions of (3.7) restricted to $(0, \infty) \times \mathcal{K}^o$.

Proposition 4.2. *For any nontrivial solution pair* $(\lambda, u) \in \mathcal{C}_n \cap (0, \infty) \times \mathcal{K}^o, n = 1, 2, \ldots,$ *it follows that* u *can be associated with a* C^2*, even, 2-periodic function. The resulting extension has minimal period* $2/n$*, and either has a maximum at* $s = 0$ *and a minimum at* $s = 1/n$ *or vice-versa. Moreover, the extension possesses reflection symmetry about the maximum and minimum locations, and is strictly monotone on* $(0, 1/n)$*.*

Proof. Given the equivalence of systems (2.23) and (4.1), we see that u possesses each of the appropriately scaled properties deduced above. So the only issue to address is the fact that $\ell = n$. We argue by contradiction: Suppose that $\ell \neq n$. Now $(2.7)_1$ insures that $u(0)$ and $u(1/\ell)$ have opposite signs. Thus, u has a single zero on $(0, 1/\ell)$, leading to precisely ℓ zeros on $(0, 1)$. But this contradicts (3.10) unless $\ell = n$. □

Recall that the signature of fracture is $H = 0$ at some point or points in $[0, \lambda]$. Referring again to (4.3) and the phase portrait in Fig. 5(b), we see that this corresponds to a closed phase curve containing the origin. As in the previous section, the sub-branch $\mathcal{C}_n^o$ is defined as the component of $\mathcal{C}_n \cap (0, \infty) \times \mathcal{K}^o$ that contains the bifurcation point $(\lambda_n, 0), n = 1, 2, \ldots$

Theorem 4.3. *Each of the sub-branches,* $\mathcal{C}_n^o, n = 1, 2, \ldots,$ *is bounded in* $(0, \infty) \times \mathcal{H}$*.*

Proof. We argue by contradiction; suppose that $\mathcal{C}_n^o$ is unbounded. The bound $(2.24)_3$ then implies there is a sequence $\{(\lambda_j, u_j)\} \subset \mathcal{C}_n^o$ with $\lambda_j \to \infty$. By (2.5) we then have a sequence of solutions $\{(\lambda_j, H_j)\}$ of (4.1) on $(a_*, b_*) = (0, \lambda_j)$ such that

$$H_j(y) = [1 + u_j(y/\lambda_j)]/\lambda_j > 0 \;\text{ on }\; [0, \lambda_j], \tag{4.5}$$

with the sequence of centers (4.4) satisfying

$$\alpha_j = 1/\lambda_j \searrow 0. \tag{4.6}$$

Since H_j is positive, (4.6) implies that the amplitude of the "oscillation" must also approach zero. Indeed, set $0 < \delta_j := \min_{y\in[0,\lambda]} H^j(y) < \alpha_j = 1/\lambda_j$. The phase curve (4.3) containing the point $(0, \delta_j)$ is then given by

$$\frac{\varepsilon}{2}(H')^2 + \varpi_j H - W^*(H) = \Gamma_j, \tag{4.7}$$

where $\Gamma_j = \varpi_j\delta_j - W^*(\delta_j)$ and $\varpi_j = \dot{W}^*(\alpha_j)$, cf. (4.2) and Fig. 5a. From (4.2) and (4.6), we have $\varpi_j = \dot{W}^*(\alpha_j) \nearrow \dot{W}^*(0) = \gamma$ and $W^*(\delta_j) \to W^*(0) = 0$. Thus, $\Gamma_j \searrow 0$ as $j \to \infty$. But (4.3) with $\varpi = \gamma$ and $\Gamma = 0$ gives only the "equilibrium" $H \equiv 0$. Thus, for all sufficiently large j, (4.7) yields a small closed orbit indicating a bounded minimal period. But this contradicts the previous observation (above Proposition 4.2) that the minimal period of the solution H_j is given by $T_j = 2\lambda_j/n \ \to \infty$ as $j \to \infty$. □

Proposition 3.2 and Theorem 4.3 immediately imply $\mathcal{C}_n^o \neq \mathcal{C}_n, n = 1, 2, \ldots$, and we also deduce

Corollary 4.4. *The closure of each sub-branch contains a fractured solution, viz., there is* $(\lambda_n^*, u_n^*) \in \overline{\mathcal{C}_n^o}$ *with* $u_n^* \in \partial\mathcal{K}$ *and* $\lambda_n^* > 1$, *for* $n = 1, 2, \ldots$.

Proof. Consider sequences $\{(\lambda_j, u_j)\} \subset \mathcal{C}_n^o$ and $\left\{(\tilde{\lambda}_j, \tilde{u}_j)\right\} \subset \mathcal{C}_n\backslash\mathcal{C}_n^o$, each converging to $(\lambda_n^*, u_n^*) \in \mathcal{C}_n$. Then $(\lambda_n^*, u_n^*) \in \overline{\mathcal{C}_n^0} \cap (\mathcal{C}_n\backslash\mathcal{C}_n^0)$. The first observation made in Remarks 4.1 shows that $\lambda_n^* > 1$. □

For each $(\lambda_n^*, u_n^*) \in \overline{\mathcal{C}_n^o}$ as above, it is clear that u_n^* is also characterized as in Proposition 4.2, with a minimum value of -1. Let H_n^* denote its rescaling via (2.5), which corresponds to a closed phase curve containing the origin in Fig. 6b. In view of Proposition 3.2, H_n^* can be associated with a C^2 even function of period $2\lambda_n^*/n$, having either a maximum at $y = 0$ and a minimum at $y = \lambda_n^*/n$ or vice-versa. In addition, H_n^* is strictly monotone on $(0, \lambda_n^*/n)$ and possesses reflection symmetry at the maximum and minimum locations. Observe that fracture ($H_n^* = 0$) occurs only at a finite number of points in $[0, \lambda_n^*]$.

We claim that all other fractured or broken solutions for $\lambda > \lambda_n^*$, denoted $H_{n,\lambda}$, can be constructed from H_n^* via a "cut and paste" procedure: $H_{n,\lambda} \equiv 0$ is inserted on a set of measure $\lambda - \lambda_n^*$ at locations where H_n^* possesses zeros, while $H_{n,\lambda}$ maintains the values of H_n^*, but now translated on n sub-intervals intervals, each of length λ_n^*/n. There are only two such possibilities when $n = 1$. This follows from the fact that H_1^* has only one zero on $[0, \lambda_*]$, which, due to monotonicity, occurs at one of the two ends of the interval. For example, if $H_1^*(\lambda_1^*) = 0$, then

$$H_{1,\lambda}(y) = \begin{cases} H_1^*(y), & y \in [0, \lambda_1^*], \\ 0, & y \in (\lambda_1^*, \lambda]. \end{cases} \tag{4.8}$$

For each $n \geq 2$, there are multiple locations where open sets of total measure $\lambda - \lambda_n^*$ can be inserted. Hence, there are uncountably many, measure-theoretic equivalent ways to carry out the latter construction. We now show that the above construction is rigorous.

Theorem 4.5. *If* $(\lambda, u) \in \mathcal{C}_n \backslash \overline{\mathcal{C}_n^o}, n = 1, 2, \ldots,$ *then there are precisely* n *open sub-intervals, each of length* $\lambda_n^*/n\lambda, \lambda > \lambda_n^*,$ *over which* u *is monotone with* $u > -1$ *, and* $u \equiv -1$ *on the complementary set of measure* $1 - (\lambda_n^*/\lambda)$*, where* $(\lambda_n^*, u_n^*) \in \overline{\mathcal{C}_n^o}$ *is defined in Corollary 4.4. Moreover, if the broken part of the solution, viz.,* $u \equiv -1,$ *is excised, then* u *can be associated with a* C^2 *even,* $2/n$ *-periodic function, viz., with* u_n^**.*

Proof. Consider the proposed construction of a broken solution as described above. Then H_n^* satisfies (4.1) on each of the n sub-intervals, of length λ_n^*/n, contained in $[0, \lambda]$, with $H_{n,\lambda} \equiv 0$ on the complement. Rescaling according to (2.5) then then yields

$$u_{n,\lambda}(s) := \begin{cases} \lambda \tilde{H}_n^*(\lambda s) - 1, & s \in \mathcal{G}, \\ -1, & s \in \mathcal{B}, \end{cases}$$

where $|\mathcal{B}| = 1 - (\lambda_n^*/\lambda)$, $\mathcal{G}$ is the union of n intervals, each of length $\lambda_n^*/n\lambda$, and $\tilde{H}_n^*$ represents the translated portions of $\lambda H_n^*(\lambda \cdot) - 1$ on $\mathcal{G}_u$. For example, the rescaling of (4.8) reads

$$u_{1,\lambda}(s) = \begin{cases} \lambda H_1^*(\lambda s) - 1, & s \in [0, \lambda_1^*/\lambda], \\ -1, & s \in (\lambda_1^*/\lambda, 1]. \end{cases} \tag{4.9}$$

Clearly $u_{n,\lambda} \in \mathcal{K}$ satisfies (2.23) on each of the n sub-intervals comprising $\mathcal{G}$, with $b - a = \lambda_n^*/n\lambda$ and $\mu = \lambda^3 \varpi$. We claim that $u_{n,\lambda}$ satisfies (2.18), which is equivalent to (2.11): First decompose the left side of (2.18) evaluated at $u_{n,\lambda}$ into the sum of two integrals over $\mathcal{G}$ and $\mathcal{B}$. The former vanishes by construction, and the integral over $\mathcal{B}$ leads directly to

$$(\lambda^3 \dot{W}^*(0) - \mu) \int_{\mathcal{B}} \psi dx = \lambda^3 (\gamma - \varpi) \int_{\mathcal{B}} \psi dx. \tag{4.10}$$

From the development in Section 4, we have $\gamma > \varpi$, cf. Fig. 6. Accordingly (4.10) is positive for all test functions $\psi \in H^1(0,1)$ with $\psi \geq 0$ on $\mathcal{B}$, which proves the claim. Clearly $(\lambda, u_{n,\lambda})$ is connected to (λ_n^*, u_n^*), and thus, $(\lambda, u_{n,\lambda}) \in \mathcal{C}_n$ for all $\lambda > \lambda_n^*$. Finally, we can associate each such $u_{n,\lambda}$ with $u_n^*(s) = \lambda H_n^*(\lambda s) - 1$ on $\mathbb{R}(\bmod 2/n)$ via excision. □

We finish this section with some stability/instability results. We adopt the usual energy criterion for stability, viz., an equilibrium solution is *stable* if it renders the potential energy a minimum; it is *locally stable* if it renders the potential energy a local minimum; if the potential energy is not a minimum (neither local not global), the equilibrium is unstable. Referring to (2.6), it is not hard to show that $V_\varepsilon[\lambda, \cdot]$ is a C^2 functional on $\mathcal{H}$. Thus, we may rigorously employ the second-derivative test (second variation) to determine local minima or to demonstrate instability. For any solution of (2.11) or equivalently (3.7), the second variation takes the form

$$\delta^2 V_\varepsilon[\lambda, u; \eta] := \frac{d^2}{d\tau^2} V_\varepsilon[\lambda, u + \tau\eta]|_{\tau=0} = \int_0^1 [\varepsilon(\eta')^2 + \lambda^2 \ddot{W}^*([1+u]/\lambda)\eta^2] ds, \tag{4.11}$$

for all $\eta \in \mathcal{H}$. We first consider the trivial solution.

Proposition 4.6. *The trivial solution $u \equiv 0$ is locally stable for all $\lambda \in (0, \lambda_1)$ and unstable for all $\lambda \in (\lambda_1, \infty)$, where λ_1 is the smallest root of (3.3), i.e., $(\lambda_1, 0) \in (0, \infty) \times \mathcal{H}$ is the first bifurcation point, cf. Theorem 3.1.*

Proof. Evaluating (4.11) at $u \equiv 0$ gives

$$\delta^2 V_\varepsilon[\lambda, 0; \eta] = \int_0^1 [\varepsilon(\eta')^2 + \lambda^2 \ddot{W}^*(1/\lambda)\eta^2] ds, \tag{4.12}$$

for all variations $\eta \in \mathcal{H}$. Next we employ the sharp Poincaré inequality

$$\int_0^1 (\eta')^2 ds \geq \pi^2 \int_0^1 \eta^2 ds, \tag{4.13}$$

where π^2 is the first eigenvalue of the operator $-\eta''$ on $[0, 1]$, subject to conditions $(3.1)_{2,3}$. Then (4.12), (4.13) lead to

$$\delta^2 V_\varepsilon[\lambda, 0; \eta] \geq [\varepsilon\pi^2 + \lambda^2 \ddot{W}^*(1/\lambda)] \int_0^1 \eta^2 ds. \tag{4.14}$$

In view of (3.3) with $n = 1$, and from the graph of $-\ddot{W}^*(\cdot)$, we conclude that $\varepsilon\pi^2/\lambda^2 > -\ddot{W}^*(1/\lambda)$ for all $1/\lambda > 1/\lambda_1$, cf. (1.4) and Fig. 5b. Of course this implies that (4.14) is positive for all $\lambda \in (0, \lambda_1)$ and $\eta \in \mathcal{H}$.

For any $\lambda > \lambda_k$, choose the admissible test functions $\eta_\ell := \cos(\ell\pi s)$, for $\ell = 1, 2, \ldots, k$. Then

$$\delta^2 V_\varepsilon[\lambda, 0; \eta_\ell] = [\varepsilon\ell^2\pi^2 + \lambda^2 \ddot{W}^*(1/\lambda)]/2.$$

Again, from (3.3) and the graph of $\ddot{W}^*(\cdot)$, we see that $\varepsilon\ell^2\pi^2/\lambda^2 < -\ddot{W}^*(1/\lambda)$, implying that $\delta^2 V_\varepsilon[\lambda, 0; \eta_\ell] < 0$, for $\ell = 1, 2, \ldots, k$. □

Next, we borrow a construction from [13] to show that the "higher-mode" global solution branches are all unstable.

Proposition 4.7. *For any $(\lambda, u) \in \mathcal{C}_n$, $n = 2, 3, \ldots$, the second variation (4.11) is strictly negative at some $\eta \in \mathcal{H}$, i.e., u is unstable.*

Proof. In view of Proposition 4.6, we need only consider $u \neq 0$. Let u be associated with an even, $(2\lambda_*/n\lambda)-$ periodic function: If $u \in \mathcal{K}^o$, then $\lambda_* = \lambda$, cf. Proposition 4.2. If $u \notin \mathcal{K}^o$, then $\lambda_* = \lambda_n^*$, cf. Theorem 4.5. In any case, for $n \geq 2$ there is an interval $(a, b) \subset (-1, 1)$, with $b - a = 2\lambda_*/n\lambda$, such that (2.23) is valid. Theorem 4.5 implies that u is reflection-symmetric with respect to the midpoint of (a, b). Without loss of generality, we assume $a = 0$. Note that (2.23) implies (via bootstrap) that

$$\varepsilon u''' \equiv \lambda^2 \ddot{W}^*\left([1 + u]/\lambda\right) u'. \tag{4.15}$$

Next, define

$$\varphi(s) := \begin{cases} u'(s), & s \in [0, 2\lambda^*/n\lambda], \\ 0, & \text{otherwise.} \end{cases}$$

By virtue of Theorem 4.5, we note that u' can be associated with an odd, $(2\lambda_*/n\lambda)$-periodic function. Accordingly, $\int_0^1 \varphi ds = 0$, and thus $\varphi \in \mathcal{H}$. Now define the admissible variation

$$\eta(s) := \phi(s) + \tau\psi(s), \tag{4.16}$$

where ψ is any function in $\mathcal{H}$ such that $\psi(0) = 1, \psi \equiv 0$ on $[2\lambda_*/n\lambda, 1]$, and τ is a small parameter. On substituting (4.16) into (4.11), we obtain

$$\begin{aligned}\delta^2 V_\varepsilon[\lambda, u; \eta] = \textstyle\int_0^b [\varepsilon(u'')^2 + \lambda^2 \ddot{W}^*([1+u]/\lambda)(u')^2]ds \\ + 2\tau \textstyle\int_0^b [\varepsilon u''\psi' + \lambda^2 \ddot{W}^*([1+u]/\lambda)u'\psi]ds + O(\tau^2),\end{aligned}$$

where $b = 2\lambda_*/n\lambda$. Then employing (4.15), we find

$$\delta^2 V_\varepsilon[\lambda, u; \eta] = -2\varepsilon\tau u''(0) + O(\tau^2).$$

Finally, since u is a non-constant solution, we have $u''(0) \neq 0$. Thus, (4.11) is negative for $|\tau|$ sufficiently small. □

5. Effective Macroscopic Behavior

In this section we interpret our results in terms of the conventional Lagrangian description, as discussed in Section 1. Taking the point of view of [14], our goal is to obtain the effective or macroscopic stress-stretch diagram based on the global solutions obtained. This is an alternative global bifurcation diagram. In view of Propositions 4.6 and 4.7, it is enough to consider only the trivial solution and the first global branch $\mathcal{C}_1$.

Presuming $H > 0$, we first express (2.3), $(2.4)_1$ in terms of the deformation gradient

$$F(x) := f'(x) = 1/H(f(x)). \tag{5.1}$$

Recalling $y = f(x) \Leftrightarrow x = h(y)$, we likewise have

$$H(y) = h'(y) = 1/F(h(y)). \tag{5.2}$$

By the chain rule and the change-of-variable formula, we find that

$$H'(f(x)) = -F'(x)/(F(x))^3, \tag{5.3}$$

and the total energy becomes [10]

$$\tilde{E}_\varepsilon[F] = \int_0^1 \left[\frac{\varepsilon}{2}\frac{(F')^2}{F^5} + W(F)\right] dx, \tag{5.4}$$

subject to

$$\int_0^1 F dx = \lambda. \tag{5.5}$$

The Euler-Lagrange equation for (5.4), (5.5) is readily obtained:

$$-\varepsilon\left[\left(\frac{F'}{F^5}\right)' + \frac{5}{2}\left(\frac{F'}{F^3}\right)^2\right] + \dot{W}(F) = \sigma \text{ on } (0,1). \tag{5.6}$$

where the multiplier σ, enforcing (5.5), represents the constant stress carried by the bar. Indeed, along the homogeneous solution $F \equiv \lambda$ we obtain the first-gradient constitutive law

$$\sigma = \dot{W}(\lambda), \tag{5.7}$$

whose graph, in view of (1.3) and Fig. 2a, is depicted (blue curve) in Fig. 4. Using (5.1)-(5.3) and the chain rule, it is not hard to see that (5.6) is equivalent to

$$\sigma = \varepsilon[H''H - (H')^2/2] + W^*(H) - H\dot{W}^*(H) \text{ on } (0,\lambda), \tag{5.8}$$

where we have also employed (1.1). From (4.1) we deduce

$$\varepsilon H''H = H[\dot{W}^*(H) - \varpi], \tag{5.9}$$

and this together with (5.8) shows that the constant of integration appearing in (4.3) is, in fact, the negative of the stress, viz.,

$$\sigma = -\Gamma. \tag{5.10}$$

Theorem 5.1. *If $(\lambda, u) \in \mathcal{C}_1 \backslash \mathcal{C}_1^o$, then the stress σ in* (5.8) *vanishes on that solution, i.e., the fractured bar carries no stress.*

Proof. Recall from the discussion above (4.8) that fracture occurs at one of the two ends of the bar; without loss of generality, we presume that u is characterized by (4.8), (4.9). Then $u(\lambda_1^*/\lambda) = -1 \Leftrightarrow H_1^*(\lambda_1^*) = 0$, and $u'({\lambda_1}^*/\lambda) = 0 \Leftrightarrow H_1^{*\prime}(\lambda_1^*) = 0$. Now (4.3) is valid for $0 \le \lambda \le \lambda_1^*$; in particular, at $y = \lambda_1^*$, we obtain $\Gamma = -\sigma = W^*(0) - \varpi \cdot 0 = 0$, cf. (1.5). □

The bounded solution branch $\overline{\mathcal{C}_1^o}$ connects the bifurcation point $(\lambda_1, 0)$ to the fracture point $(\lambda_*, u_*) := (\lambda_1^*, u_1^*)$, cf. Corollary 4.4. Hence, with $\lambda = f(1)$ playing the role of macroscopic stretch, the projection of $\overline{\mathcal{C}_1^o}$ onto the (λ, σ) plane,

$$\mathcal{T} = \{(\lambda, \sigma) \in \mathbb{R}^2 : (\lambda, u) \in \overline{\mathcal{C}_1^o} : \sigma \text{ satisfies (5.6) for } H \text{ as in (2.5)}\} \tag{5.11}$$

connects $(\lambda_1, \dot{W}(\lambda_1))$ to $(\lambda_*, 0)$. An example for a specific choice of W^* (details at the end of this section) is shown in Fig. 4, in which, for $\varepsilon = 2/49$, $\mathcal{T}$ is the orange curve, connecting the orange bifurcation point $(\lambda_1, \dot{W}(\lambda_1))$ to the black fracture point $(\lambda_*, 0)$. The remaining part $\mathcal{C}_1 \backslash \mathcal{C}_1^o$ consists of broken (fractured) solutions of the form (4.8) with an opened crack; it projects onto the ray

$$\mathcal{F} = \{(\lambda, 0) : \lambda \ge \lambda_*\}. \tag{5.12}$$

In the example of Fig. 4, for $\varepsilon = 2/49$, $\mathcal{F}$ is the part of the horizontal axis to the right of the black point.

We can say something about the stability of the component of the first branch consisting of broken solutions at this general stage.

Theorem 5.2. *There exits $\lambda_m < \infty$, such that, for every $(\lambda, u) \in \mathcal{C}_1 \backslash \mathcal{C}_1^o$ with $\lambda > \lambda_m$, the broken solution u is not only the only stable solution, but also the global minimizer of $V_\varepsilon[\lambda, \cdot]$.*

Proof. This follows by process of elimination: According to Proposition 4.6, the trivial solution $u \equiv 0$ is unstable for all $\lambda \in (\lambda_1, \infty)$, and Proposition 4.7 implies that all higher-mode solutions are unstable. Moreover, the proof of Theorem 4.3 implies that there are no monotone, strictly positive solutions $H > 0$ on $[0, \lambda]$ for $\lambda > \lambda_m$, where $\lambda_m < \infty$ is some positive constant. Hence for fixed $\lambda > \lambda_m$, the only potentially stable solutions are given by (4.9) and its anti-symmetric version generated by $u(s) \to u(1-s)$. Indeed, the phase-plane construction (4.8) demonstrates that there are no other possibilities for solutions with a single break. We then infer the result from Proposition 2.1. □

Remark 5.3. *After the bar breaks at λ_*, we can continue pulling the broken end $y = \lambda_*$ further to any $\lambda > \lambda_*$, cf.* (4.8)*. The interval $\lambda_* < y < \lambda$ is "aether" or vacuum $H = 0$ or "$F = \infty$" namely a displacement discontinuity, known as the crack-opening displacement. See the discussion pertaining to* (1.2)*. Here, broken solutions involve a two-phase inverse deformation, with the opened crack, $\lambda_* < y < \lambda$ in the broken phase, or the energy well at $H = 0$ in Fig. 2b. The rest of the deformed bar is in the unbroken phase (convex well containing $H = 1$) with a transition layer in between, whose size depends on ε. Despite this being a "diffuse interface model" due to higher gradients, the crack faces (boundaries of the $H = 0$ phase) are sharply delineated, in contrast to the diffuse cracks in damage or phase field models* [5]*. This is due to the unilateral constraint.*

Remark 5.4. *Theorems 5.1 and 5.2 imply that the bar breaks at a finite macroscopic stretch, at most λ_m, beyond which the stress (of the only stable solution) vanishes. This is somewhat different than the behavior predicted by various nonlocal or cohesive zone models* [6, 19]*, where, for fracture, the stress appears to approach zero only as the stretch goes to infinity. Our result agrees with the discrete model* [17]*, where however it is assumed that the constituent springs break (the force vanishes) at finite stretch. In contrast, our the underlying stress-stretch law is not restricted to vanish at finite homogeneous stretch. Here stress vanishes at finite average stretch due to bifurcation.*

In order to characterize the projection $\mathcal{T}$ (5.11) more explicitly, we turn to the methodology of Carr, Gurtin & Slemrod[13]. For $0 \le a < b < 1$ and $z \ge 0$, let

$$U(z, a, b) = W^*(z) - \varpi(a, b)z + \Gamma(a, b), \tag{5.13}$$

where

$$\varpi(a, b) = \frac{W^*(b) - W^*(a)}{b - a}, \qquad \Gamma(a, b) = \varpi(a, b)a - W^*(a), \tag{5.14}$$

and (formally) define

$$g_0(a, b) = \int_a^b \frac{1}{\sqrt{U(z, a, b)}} dz, \quad g_1(a, b) = \int_a^b \frac{z}{\sqrt{U(z, a, b)}} dz \tag{5.15}$$

Proposition 5.5. *(i) Suppose $(\lambda, u) \in \overline{\mathcal{C}_1^o}$ (the first bifurcating sub-branch up to fracture) with $H(y)$ as in* (2.5)*. Let $H(0) = H_2$ and $H(\lambda) = H_1$. Then these satisfy*

$$0 \le H_1 < \kappa, \quad H_1 < H_2 < 1, \tag{5.16}$$

$$U(H, H_1, H_2) > 0 \quad \forall H \in (H_1, H_2), \tag{5.17}$$

$$\sqrt{\frac{\varepsilon}{2}}g_0(H_1,H_2)=\lambda,\qquad \sqrt{\frac{\varepsilon}{2}}g_1(H_1,H_2)=1. \tag{5.18}$$

Moreover the stress σ from (5.6) *is given by*

$$\sigma = W^*(H_1)-\varpi(H_1,H_2)H_1 \tag{5.19}$$

Conversely, suppose H_1, H_2 abide by (5.16), (5.17) *and satisfy* $(5.18)_2$. *Define λ by* $(5.18)_1$. *Then there is $H:[0,\lambda]\to[0,1]$ with $H(0)=H_2$ and $H(\lambda)=H_1$, such that the corresponding $(\lambda,u)\in\overline{\mathcal{C}_1^o}$. The inverse of this H is given by*

$$\hat{y}(H)=\sqrt{\frac{\varepsilon}{2}}\int_H^{H_2}\frac{1}{\sqrt{U(z,H_1,H_2)}}dz \tag{5.20}$$

for $H\in(H_1,H_2)$. The projection (5.11) *of the corresponding (λ,u) onto the stress-stretch plane is $(\lambda,\sigma)\in\mathcal{T}$ with λ given by* $(5.18)_1$ *and σ given by* (5.19).
(ii) Setting $H_1=0$ in part (i) above gives the fracture point (λ_*,u_*). In particular, the fracture stretch

$$\lambda_*=\sqrt{\frac{\varepsilon}{2}}g_0(0,H_2),\quad \textit{where } H_2 \textit{ is a root of } \sqrt{\frac{\varepsilon}{2}}g_1(0,H_2)=1,$$

whereas the corresponding stress $\sigma_*=0$.
(iii) The projection $\mathcal{T}$ in (5.11) *is located to the right of the rising branch of the stress-stretch curve, $\{(\lambda,\dot{W}(\lambda)):0<\lambda<1/\kappa\}$, namely,*

$$(\lambda,\sigma)\in\mathcal{T}\implies 0\le\sigma<\dot{W}(1/\kappa),\quad \lambda>\lambda_\sigma, \tag{5.21}$$

where λ_σ is the unique solution of $\dot{W}(\lambda_\sigma)=\sigma$ in $[1,1/\kappa]$. Moreover, as $\varepsilon\to 0$, $\mathcal{T}$ approaches the rising branch of the stress-stretch curve in the following sense. For fixed σ with $(\lambda,\sigma)\in\mathcal{T}$,

$$\lambda\searrow\lambda_\sigma\quad \textit{as } \varepsilon\searrow 0. \tag{5.22}$$

In particular, the fracture stretch $\lambda_*\searrow 1$ as $\varepsilon\searrow 0$.

Proof. By hypothesis, Proposition 4.2 with $n=1$ and the phase portrait (see discussion leading to (4.4)), H is strictly monotone on $[0,\lambda]$ and $H'(y)\neq 0$ except at $y=0,\ \lambda$. Thus (4.3) and the natural boundary conditions $H'(0)=H'(\lambda)=0$ from $(2.14)_2$, imply that $W^*(H)-\varpi H+\Gamma=0$ for $H=H(\lambda)=:H_1$ and $H=H(0)=:H_2$, and >0 for $H\in(H_1,H_2)$. This in turn shows that

$$W^*(H)-\varpi H+\Gamma=U(H,H_1,H_2) \tag{5.23}$$

cf. (5.13), (5.14), and that (5.17) holds, whereas $U(H_i,H_1,H_2)=0$ for $i=1,2$. This means that the straight line $\varpi H-\Gamma$ intersects the graph of $W^*(\cdot)$ at H_1 and H_2, and is below it in between. Because of (2.2), this is only possible if (5.16) holds. Substituting (5.23) in (4.3), solving for H' and keeping the negative of the two solutions (the other giving equivalent results) we infer

$$H'(y)=-\sqrt{(2/\varepsilon)\,U(H(y),H_1,H_2)},\quad y\in[0,\lambda] \tag{5.24}$$

This can be solved for the inverse $y = \hat{y}(H)$ of $H(y)$, noting that $\hat{y}(H_2) = 0$, yielding (5.20). Using the latter, the requirement that $\hat{y}(H_1) = \lambda$ then gives the first of (5.18), while the integral constraint (2.4) reduces to the second of (5.18) after changing variables from y to H. Also, (5.19) follows from (5.10) and (5.14).

To show the converse, suppose $H(y)$ is a solution of (5.24) with $H(0) = H_2$; by (5.17) it is monotone. Define $\hat{y}$ from (5.20). Then it is the inverse of $H(y)$, and $(5.18)_1$ implies that $\hat{y}(H_1) = \lambda$. Hence $H(0) = H_2$, $H(\lambda) = H_1$ and $(5.18)_2$ ensures the integral constraint (2.4), while (5.24) implies (4.3). As a result the corresponding $(\lambda, u) \in \overline{\mathcal{C}_1^o}$.

Part (ii) is immediate, after setting $H_1 = 0$ in (5.18) and (5.19), recalling that $W^*(0) = 0$.

To show (iii), we note that the mapping $(H_1, H_2) \mapsto (\varpi, \Gamma)$ defined by (5.14) is one-to-one on the set of (H_1, H_2) satisfying (5.16) and (5.17) [13]. We then rewrite

$$g_i(H_1, H_2) = G_i(\varpi, \Gamma) = G_i(\varpi, -\sigma) \tag{5.25}$$

for $i = 0, 1$, in view of (5.10). For fixed $\sigma \in [0, \dot{W}(1/\kappa))$ there is an interval of ϖ values for which the chord $\varpi H + \sigma$ intersects the graph of $W^*(\cdot)$ at two points $H_1 < H_2$, and is below it in-between. This happens if and only if $\varpi_\sigma < \varpi < \varpi^\sigma$ where $\varpi^\sigma := \dot{W}^*(H^\sigma) > \varpi_\sigma := \dot{W}^*(H_\sigma)$ are slopes of rays through the point $(0, \sigma)$ and tangent to the graph of W^* at H^σ and H_σ, respectively. As a result, using (1.1) and results from [8],

$$1/H_\sigma = \lambda_\sigma := \text{the unique solution of } \dot{W}(\lambda_\sigma) = \sigma \text{ in } [1, 1/\kappa] \tag{5.26}$$

Because of (5.5), we have $\lambda > 1/H_2$. From (2.2) it follows that $H_\sigma > H_2$. As a result, $\lambda > \lambda_\sigma$. Also, if $\sigma \geq \dot{W}(1/\kappa)$, there can be at most one intersection, so the only possible $(\lambda, \sigma) \in \mathcal{T}$ is the bifurcation point $(\lambda_1, \dot{W}(\lambda_1))$. But since $\lambda_1 > 1/\kappa$, $\sigma_1 = \dot{W}(\lambda_1) < \dot{W}(1/\kappa)$, so if if $\sigma \geq \dot{W}(1/\kappa)$, then $(\lambda, \sigma) \notin \mathcal{T}$. This confirms (5.21). Adapting results from [13] we have that for some constant $C > 0$,

$$G_0(\varpi, -\sigma) \sim -C \log(\varpi - \varpi_\sigma), \quad G_1(\varpi, -\sigma) \sim -H_\sigma C \log(\varpi - \varpi_\sigma), \quad \text{as } \varpi \searrow \varpi_\sigma \tag{5.27}$$

Note that $(5.18)_2$ becomes

$$G_1(\varpi, -\sigma) = \sqrt{2/\varepsilon}.$$

For ε sufficiently small this has a solution [13]

$$\varpi = \varpi_\varepsilon \sim \varpi_\sigma + e^{-C\sqrt{2/\varepsilon}} \text{ as } \varepsilon \to 0. \tag{5.28}$$

Dividing $(5.18)_1$ by $(5.18)_2$ and using (5.25)-(5.27), we find

$$\lambda = \frac{G_0(\varpi_\varepsilon, -\sigma)}{G_1(\varpi_\varepsilon, -\sigma)} \to \lambda_\sigma \text{ as } \varepsilon \to 0.$$

Together with (5.21) this confirms (5.22). □

Remark 5.6. *In the context of the original formulation, the analogues of* (5.13)-(5.18) *are due to* [13]*; see also* [6]*. For each* $H_1 \in [0, 1/\lambda_1)$*, the second of* (5.18) *is uniquely solvable for* $H_2 = \hat{H}(H_1)$*. Define*

$$\hat{\lambda}(H_1, \varepsilon) = \sqrt{\frac{\varepsilon}{2}} g_0(H_1, \hat{H}(H_1)), \quad \hat{\sigma}(H_1) = W^*(H_1) - \varpi(H_1, \hat{H}(H_1)) H_1 \tag{5.29}$$

Then the above is a parametrization of $\mathcal{T}$, cf. (5.11)*, in the (λ, σ) plane. In specific examples we (numerically) solve the second of* (5.18) *for H_2 in terms of H_1. This gives the parametrization* (5.29) *of $\mathcal{T}$.*

Next we consider some properties of stable broken solutions (of the Euler-Lagrange inequality corresponding to (2.3)) on the first branch $\mathcal{C}_1$ with the inverse stretch vanishing on an entire subinterval. Such solutions have $H = H_b(y)$ given by the right-hand side of (4.8) for $y \in [0, \lambda]$ and $\lambda > \lambda_*$ as guaranteed by Theorems 4.5 and 5.1.

Proposition 5.7. *As $\varepsilon \to 0$, the energy* (2.3) *of a broken solution H_b is*

$$E_\varepsilon[H_b] = \sqrt{\varepsilon} \int_0^1 \sqrt{2W^*(H)} dH + o(\sqrt{\varepsilon}) = \sqrt{\varepsilon} \int_1^\infty \sqrt{2W(F)/F^5} dF + o(\sqrt{\varepsilon}) \tag{5.30}$$

Proof. Modifying an argument of [13], we write the energy (2.3) of H_b as follows, observing the constraint $\int_0^\lambda H_b(y)dy = 1$, noting that $H_b = 0$ on $[\lambda_*, \lambda]$ by (4.8) and using (5.13),

$$\begin{aligned}
E_\varepsilon[H_b] &= \int_0^\lambda \Big(\frac{\varepsilon}{2} [H_b'(y)]^2 + W^*(H_b(y)) - \varpi [H_b(y) - 1/\lambda] \Big) dy \\
&= \int_0^{\lambda_*} \Big(\frac{\varepsilon}{2} [H_b'(y)]^2 + W^*(H_*(y)) - \varpi H_*(y) \Big) dy + \varpi \\
&= \int_0^{\lambda_*} \Big(\frac{\varepsilon}{2} [H_b'(y)]^2 + U(H_*(y), 0, H_2(\varepsilon) \Big) dy + \varpi(0, H_2(\varepsilon)) \\
&= \int_0^{\lambda_*} 2U(H_*(y), 0, H_2(\varepsilon)) dy + \varpi(0, H_2(\varepsilon)) \\
&= \sqrt{\varepsilon} \int_0^{H_2(\varepsilon)} \sqrt{2U(H, 0, H_2(\varepsilon))} dH + \varpi(0, H_2(\varepsilon))
\end{aligned}$$

where we have used (5.24) to obtain the fourth line above and the change of variables (5.20) from y to $H = H_b(y)$ for the fifth line. Here $H_2(\varepsilon)$ is the root of the second of (5.18) with $H_1 = 0$. As $\varepsilon \to 0$,(5.28) applies, whereas $\varpi_\sigma = 0$ because $\sigma = 0$, so that the second term above $\varpi(0, H_2(\varepsilon)) = o(\sqrt{\varepsilon})$. From (5.28) and the fact that $W^*(H) = O(H-1)^2$ as $H \to 1$, we have that $H_2(\varepsilon) = 1 + o(\sqrt{\varepsilon})$. As a result we can replace the upper limit in the integral in the last line above by 1. □

Remark 5.8. *Here there is a transition layer from H close to 1 to $H = 0$ of size approximately $\sqrt{\varepsilon}$ for small ε. In* (4.8)*, this layer occurs just to the left of the crack face $y = \lambda_*$. This is easily shown. Moreover the first formula in* (5.30) *is formally identical to the interfacial energy of a phase boundary with higher gradients* [13]*, so this energy can be interpreted as the energy cost for the creation of new surfaces, or the surface energy of fracture in the sense of Griffith* [1].

In order to gain more information concerning the stability of the first branch, the shape of its projection $\mathcal{T}$ in the (λ, σ) plane and the location of the fracture stretch λ_*, we turn to specific models for W^* and compute the first global branch of solutions.

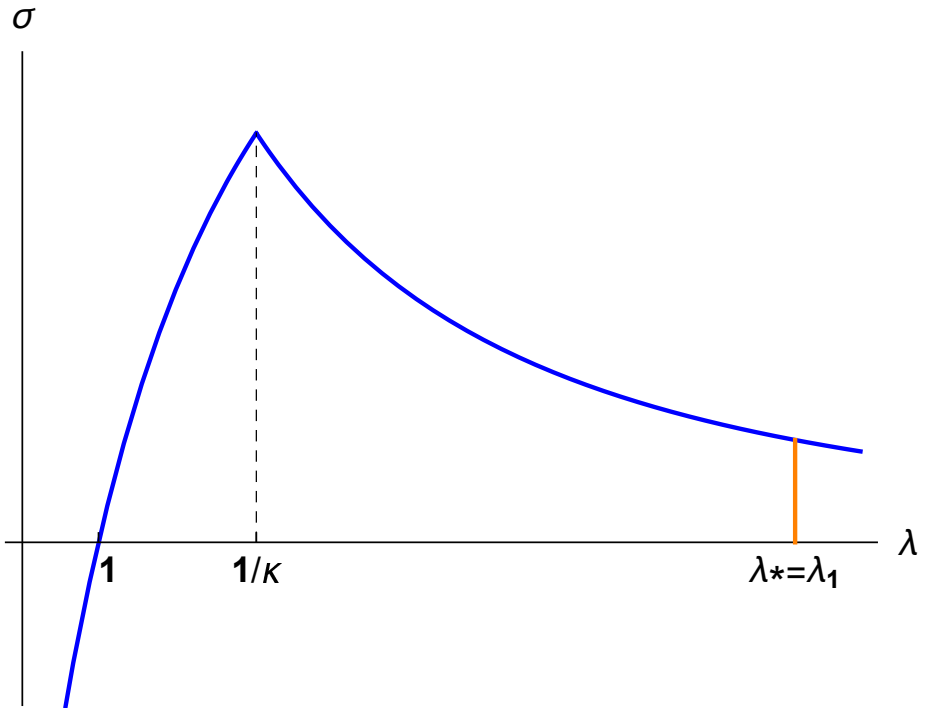


FIGURE 7. The homogeneous stress *vs* stretch trivial branch (blue) and the projection $\mathcal{T}$ (orange) of the first bifurcation branch for the special constitutive law (5.31) in Example 5.9 for $\varepsilon = 16/\pi^2$.

Example 5.9. We introduce a special W^* that is piecewise-quadratic, so that the Euler-Lagrange equation is (piecewise) linear. Let

$$\kappa = 1/\sqrt{2}, \quad d = \sqrt{2} - 1$$

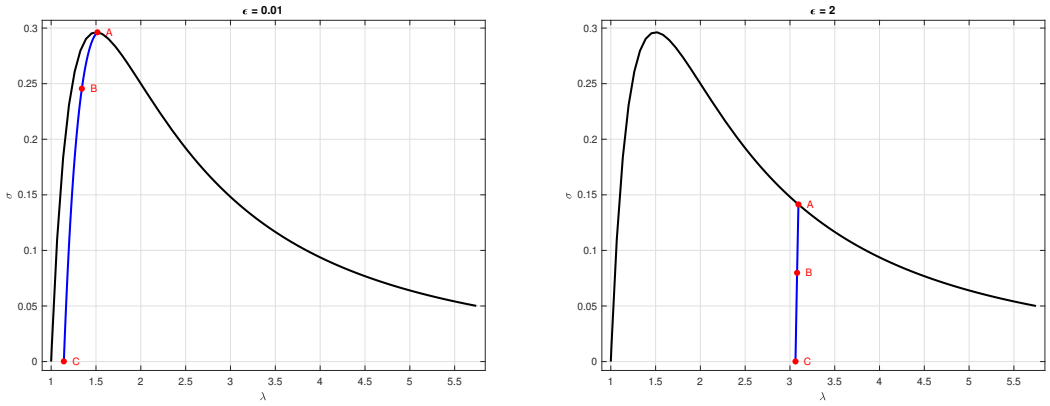
and define

$$W^*(H) = \begin{cases} d^2 - (H-d)^2, & 0 \le H \le \kappa, \\ (H-1)^2, & \kappa < H < \infty. \end{cases} \tag{5.31}$$

This abides by (2.2) except for smoothness, as it is C^1 but only piecewise C^2, but this does not affect our conclusions here. Suppose we look at solutions of (2.14) such that $0 < H(x) < \kappa$ for $0 < x < \lambda$, so that

$$-1 < u(s) < \kappa\lambda - 1, \quad s \in (0,1) \tag{5.32}$$

in (2.14) (this demands that $\lambda > 1/\kappa$). Then (2.14) becomes linear and reduces exactly to (3.1), whose solutions are $u(s) = A\cos(n\pi s)$, $0 \le s \le 1$, for some constant A, with λ restricted to satisfy (3.3), namely $\lambda = \lambda_n = n\pi\sqrt{\varepsilon/2}$. The bifurcation condition thus holds all along each branch, from $A = 0$ at bifurcation, all the way to fracture where $|A| = 1$, so that $u = -1$ at one end. The second inequality in (5.32) then asserts $\kappa\lambda \ge 2$, which is



(A) (B)

FIGURE 8. The homogeneous stress *vs* stretch trivial branch (black) and the projection $\mathcal{T}$ (blue) of the first bifurcation branch for the special constitutive law (5.36) in Example 5.10. (A) $\varepsilon = 0.01$; (B) $\varepsilon = 2$. Point A is the bifurcation point $(\lambda_1, \dot{W}(\lambda_1)$. Point C is the fracture point $(\lambda_*, 0)$.

equivalent to $\varepsilon \geq 16/\pi^2$ for $n = 1$. The projection of each of the branches on the (λ, σ) plane is a vertical line from the bifurcation point $(\lambda_n, \dot{W}^*(\lambda_n))$ on the trivial branch, all the way down to $(\lambda, \sigma) = (\lambda_n, 0)$. In particular, note that $\lambda_* = \lambda_1 = \pi\sqrt{\varepsilon/2}$ and the projection $\mathcal{T}$ of the first bifurcation branch is the orange vertical line in Fig. 7.. According to the construction (4.8), (4.9), the broken part of the branch for all $\lambda > \lambda_1$ corresponds to

$$u(s) = \begin{cases} (\lambda/\lambda_1)\cos(\lambda\pi s/\lambda_1), & s \in [0, \lambda_1/\lambda), \\ -1, & s \in [\lambda_1/\lambda, 1]. \end{cases} \tag{5.33}$$

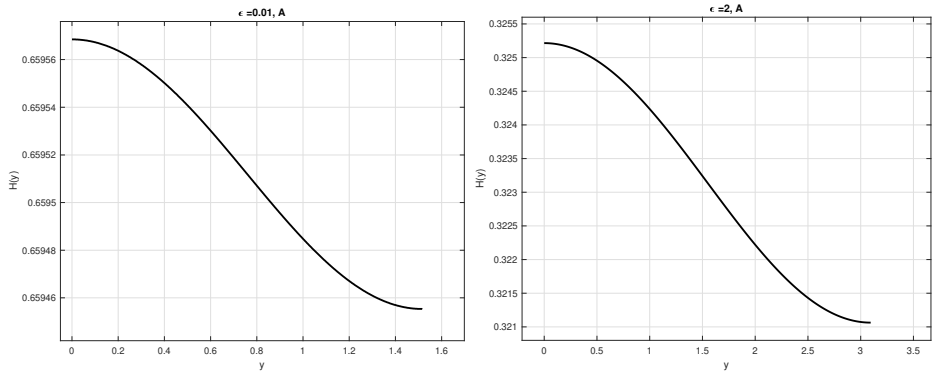
The bifurcation condition (3.3) holds along the entire branch $\mathcal{C}_1^o$ in this case, which implies that the second variation (4.11) can vanish. To see this, note that integration by parts in (4.11) yields

$$\delta^2 V_\varepsilon[\lambda, u; \eta] = \int_0^1 [-\varepsilon\eta'' + \lambda^2 \ddot{W}^*([1+u]/\lambda)\eta]\eta ds, \tag{5.34}$$

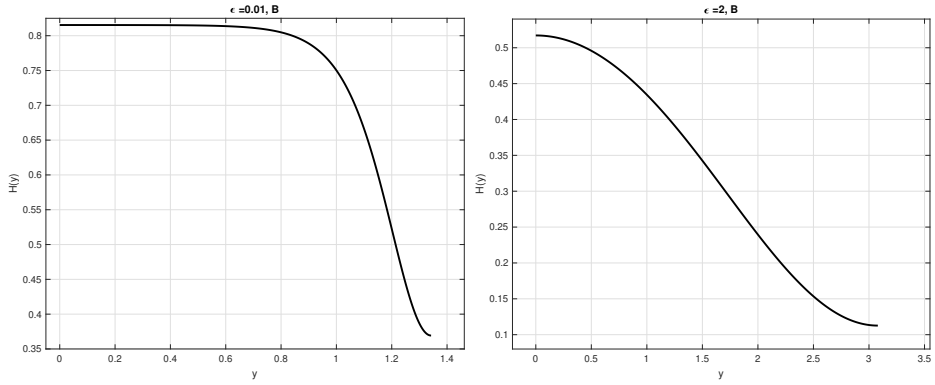
for all $\eta \in \mathcal{H}$. Here $\ddot{W}^* \equiv -2$, and the integrand vanishes at $\lambda = \lambda_1$ and $\eta(s) = \cos(\pi s)$, as already noted. In fact, we claim that the second variation is positive semi-definite: If we restrict variations to the orthogonal complement of $\text{span}\{\cos(\pi s)\}$ in $\mathcal{H}$, denoted $\tilde{\mathcal{H}}$, then the sharp Poincaré inequality (4.13) now incorporates the second eigenvalue of the operator, viz., $4\pi^2$, and for $0 < |A| \leq 1$, we obtain

$$\delta^2 V_\varepsilon[\lambda_1, A\cos(\pi s); \eta] \geq 3\varepsilon\pi^2, \tag{5.35}$$

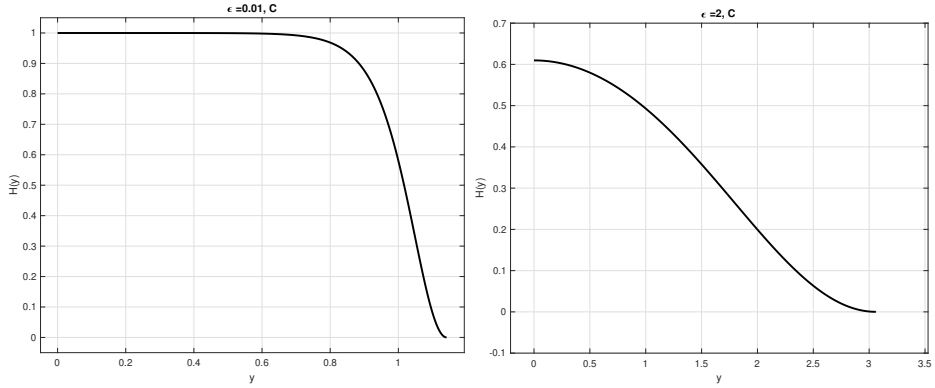
for all $\eta \in \tilde{\mathcal{H}}$. Hence, in this special case, u is locally "neutrally" stable for all $(\lambda, u) \in \overline{\mathcal{C}_1^o} \backslash \{(\lambda_1, 0)\}$.



(A)



(B)



(C)

FIGURE 9. Bifurcated first-branch solutions $H(y)$ *vs* y from points A, B, C along the first-branch projection in Fig. 8 for the special constitutive law (5.36) in Example 5.10. Left column: $\varepsilon = 0.01$; right column: $\varepsilon = 2$. (A) near the bifurcation point; note small variation of H. (B) At an intermediate point along the sub-branch. (C) at the fracture point.

Example 5.10. Next we consider

$$W(F) = (1 - 1/F)^2 \implies W^*(H) = H(1-H)^2, \tag{5.36}$$

which follows from from (1.1) and also fulfills our hypotheses (2.2). See Fig. 2 for W and W^*. It is enough to solve (2.14) in order to compute the sub-branch $\mathcal{C}_1^o$ and its projection onto the (λ, σ) plane. For that purpose, we used the bifurcation/continuation software AUTO [16]. In Fig. 8a and Fig. 8b we depict the computational results for the cases $\varepsilon = 0.01$ and $\varepsilon = 2$, respectively. The computed values of λ_* in these two cases are approximately 1.14 and 3.06, respectively. In each of the two figures we specify three points along the curve at which the corresponding computed solution configurations are depicted in Fig. 9. For $\varepsilon = 0.01$, observe the development of a transition layer from $H \approx 1$ to $H \approx 0$ on the right-hand side of the bar in Fig. 9b and Fig. 9c. Fracture occurs at the rightmost point $y = \lambda_*$ where $H(\lambda_*) = 0$ in Fig. 9c. .

We also use the semi-analytical solution of Proposition 5.5(i). We numerically compute the set of (H_1, H_2) satisfying $(5.18)_2$ and (5.16). We then compute the corresponding $(\lambda, \sigma) \in \mathcal{T}$ from $(5.18)_2$ and (5.19). The projection $\mathcal{T}$ of the first branch so obtained is shown in Fig. 4 for three values of ε. As predicted by part (ii) of Proposition 5.5, as ε decreases, $\mathcal{T}$ tends towards the rising branch of the stress-stretch curve.

Remark 5.11. *In both the above examples, a quasistatic increase of average stretch λ (equivalently the end displacement of the bar) will cause a sudden drop of the stress σ to zero upon fracture. This will occur at some stretch level that is equal to the bifurcation point λ_1 in Example 5.9, or some value between $\lambda_a st$ and λ_1 for Example 5.10, depending on one's favorite notion of stability (local vs global), and perhaps ambient disturbances or imperfections. Many nonlocal or cohesive zone models* [6, 19] *instead predict a load drop to a positive stress, followed by a gradual asymptotic decrease to zero. In contrast a discrete model exhibits sudden drop to zero stress for long bars only, after assuming that "interatomic springs" lose force (break) at finite stretch. We do not need to assume this for our constitutive law. For shorter bars our model predicts a larger fracture stretch and a smaller stress drop to zero at fracture.*

References

[1] Alan Arnold Griffith. Vi. the phenomena of rupture and flow in solids. *Philosophical transactions of the royal society of london. Series A, containing papers of a mathematical or physical character*, 221(582-593):163–198, 1921.

[2] Grigory Isaakovich Barenblatt et al. The mathematical theory of equilibrium cracks in brittle fracture. *Advances in applied mechanics*, 7(1):55–129, 1962.

[3] Luigi Ambrosio and Andrea Braides. Energies in sbv and variational models in fracture mechanics. *Homogenization and applications to material sciences*, 9:1–22, 1997.

[4] Gilles A Francfort and J-J Marigo. Revisiting brittle fracture as an energy minimization problem. *Journal of the Mechanics and Physics of Solids*, 46(8):1319–1342, 1998.

[5] Blaise Bourdin, Gilles A Francfort, and Jean-Jacques Marigo. Numerical experiments in revisited brittle fracture. *Journal of the Mechanics and Physics of Solids*, 48(4):797–826, 2000.

[6] Nicolas Triantafyllidis and S Bardenhagen. On higher order gradient continuum theories in 1-d nonlinear elasticity. derivation from and comparison to the corresponding discrete models. *Journal of Elasticity*, 33(3):259–293, 1993.
[7] L Truskinovsky. Fracture as a phase transition. *Contemporary research in the mechanics and mathematics of materials*, pages 322–332, 1996.
[8] Richard T Shield. Inverse deformation results in finite elasticity. *Zeitschrift für angewandte Mathematik und Physik ZAMP*, 18(4):490–500, 1967.
[9] Jerald L Ericksen. Equilibrium of bars. *Journal of elasticity*, 5(3-4):191–201, 1975.
[10] Donald E Carlson and T Shield. Inverse deformation results for elastic materials. *Zeitschrift für angewandte Mathematik und Physik ZAMP*, 20(2):261–263, 1969.
[11] Phoebus Rosakis. A two-dimensional inverse-deformation approach to brittle fracture. *preprint*, 2020.
[12] Paul H Rabinowitz. Some global results for nonlinear eigenvalue problems. *Journal of functional analysis*, 7(3):487–513, 1971.
[13] Jack Carr, Morton E Gurtin, and Marshall Slemrod. Structured phase transitions on a finite interval. *Archive for Rational Mechanics and Analysis*, 86(4):317–351, 1984.
[14] AE Lifshits and Grigorii Leonidovich Rybnikov. Dissipative structures and couette flow of a nonnewtonian fluid. *Soviet Physics Doklady*, 281(5):1088–1093, 1985.
[15] Vy Khoi Le and Klaus Schmitt. *Global bifurcation in variational inequalities: applications to obstacle and unilateral problems*, volume 123. Springer Science & Business Media, 1997.
[16] EJ Doedel and BE Oldeman. Auto-07p: Continuation and bifurcation software for ordinary differential equations. *Concordia University; Montreal, Canada: 2009*, 2009.
[17] Andrea Braides, Gianni Dal Maso, and Adriana Garroni. Variational formulation of softening phenomena in fracture mechanics: The one-dimensional case. *Archive for Rational Mechanics and Analysis*, 146(1):23–58, 1999.
[18] Huajian Gao and Baohua Ji. Modeling fracture in nanomaterials via a virtual internal bond method. *Engineering Fracture Mechanics*, 70(14):1777–1791, 2003.
[19] Gianpietro Del Piero and Lev Truskinovsky. Elastic bars with cohesive energy. *Continuum Mechanics and Thermodynamics*, 21(2):141, 2009.
[20] Michael G Crandall and Paul H Rabinowitz. Nonlinear sturm-liouville eigenvalue problems and topological degree. *Journal of Mathematics and Mechanics*, 19(12):1083–1102, 1970.
[21] David Kinderlehrer and Guido Stampacchia. *An introduction to variational inequalities and their applications*. SIAM, 2000.
[22] John L Synge and Byron A Griffith. *Principles of mechanics*. McGraw-Hill, 1970.

(1) Department of Mathematics and Applied Mathematics, University of Crete, Heraklion 70013 Crete, Greece. Email: rosakis@uoc.gr

(2) Institute of Applied and Computational Mathematics, Foundation for Research and Technology-Hellas, Voutes 70013 Crete, Greece

(3) Department of Mathematics, Cornell University, Ithaca, NY 14853, USA. Email: tjh10@cornell.edu

(4) Field of Theoretical and Applied Mechanics, Cornell University, Ithaca, NY 14853, USA